CHAPTER

Presolar oxide grains 5

Larry R. Nittler, Rhonda M. Stroud
Arizona State University, Tempe, AZ, United States

1 Historical background and introduction

The 1973 discovery that calcium-aluminum-rich inclusions (CAIs) are ^{16}O-rich compared to the Earth (Clayton et al., 1973) led to the expectation that meteorites may contain presolar, stellar refractory oxide grains with isotopic compositions reflecting nuclear processes that occurred in their parent stars. Moreover, astronomical observations suggested that O-rich interstellar dust dominates the cosmos. It was thus somewhat surprising that the first bona fide presolar grains to be unambiguously identified were carbon-bearing: diamond, SiC, and graphitic C (Lewis et al., 1987; Bernatowicz et al., 1987; Tang and Anders, 1988; Amari et al., 1990) and it is now known that the CAI isotope signature reflects the bulk Solar System, not an admixture of presolar grains. Nevertheless, with the discovery of C-rich presolar grains in the acid residues of primitive meteorites, attention was soon paid to the sub-micrometer to micrometer-sized oxide grains (generally refractory phases like spinel, $MgAl_2O_4$, and alumina, Al_2O_3) in the same residues to see if any may show nucleosynthetic isotope signatures. The first direct evidence came from measurements of very fine-grained spinel separates obtained from the Murray CM chondrite using the ims-3f secondary ion mass spectrometer (SIMS; Zinner and Tang, 1988). O isotope measurements containing large numbers of individual grains revealed small excesses in ^{17}O relative to the normal range of solar system materials, suggesting that some fraction of the grains may be much more anomalous. Confirmation of this result would have to wait some 15 years for the development of the NanoSIMS ion microprobe to allow individual O isotope measurements on <200-nm-sized grains (Zinner et al., 2003). In the meantime, in 1992, Gary Huss and coworkers at Caltech reported ims-3f measurements of micron-sized Al_2O_3 grains from the Orgueil meteorite, including a grain with a large ^{26}Mg excess indicating the presence of extinct ^{26}Al at ~100 times the level believed to have been present in the early Solar System (Huss et al., 1992). These authors suggested a presolar origin for this grain, and this was dramatically confirmed 2 years later when O isotope measurements revealed the grain to have an ^{17}O/^{16}O ratio, a factor of 2.5 times higher than that of the Earth (Hutcheon et al., 1994), directly pointing to stellar nucleosynthesis. Contemporaneously with the Caltech efforts, the Washington Uni-

Presolar Grains in Extra-Terrestrial Materials. https://doi.org/10.1016/B978-0-12-821830-3.00010-3

versity group developed an automatic ion imaging system on the ims-3f to rapidly screen $^{18}O/^{16}O$ ratios of dispersed grains and identify anomalous ones (Fig. 1; Nittler et al., 1993), soon leading to the discovery of tens of presolar corundum and spinel grains in acid residues of the Murchison (CM2) and Tieschitz (H/L3) meteorites (Nittler et al., 1994). Preliminary interpretations of the grain data in terms of possible stellar sources and processes soon appeared (Huss et al., 1994; Nittler et

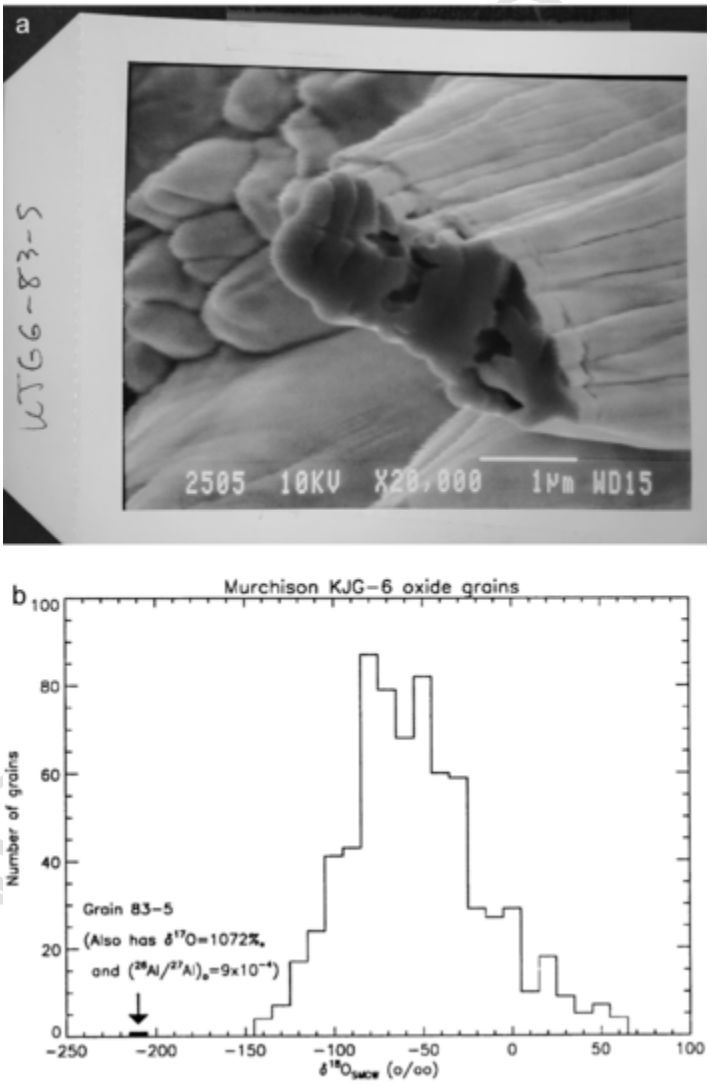

- Reproduced from Nittler, L.R., Walker, R.M., Zinner, E., Hoppe, P., Lewis, R.S., 1993. Identification of an interstellar oxide grain from the Murchison meteorite by ion imaging. Lunar Planet. Sci. XXIV, 1087–1088.

al., 1994; Wasserburg et al., 1995), and within a few years, hibonite ($CaAl_{12}O_{19}$) was added to the stable of known presolar oxide grains (Choi et al., 1999).

New ion probe technology in the early part of this century (e.g., NanoSIMS, ims-1270 with SCAPS detector) led to the discovery of the much more abundant presolar silicates in situ in interplanetary dust particles (IDPs) and meteorites (Chapter 6; Messenger et al., 2003; Nagashima et al., 2004; Nguyen and Zinner, 2004), but large numbers of presolar oxides, including many new phases and even composite presolar oxide-silicate grains, have continued to be identified and studied, both in acid residues and in situ in extraterrestrial samples to the present day. In this chapter, we review the types of known presolar oxides, their isotopic, elemental, and mineralogical compositions, and their possible stellar origins. Because there is strong overlap in their compositions and sources with presolar silicates, there is some overlap in material between this chapter and Chapter 6.

2 What is a presolar oxide grain?

Strictly speaking, a *presolar* grain is a dust particle that existed in the interstellar molecular cloud from which our Sun and planets began to form some 4.6 billion years ago and continues to exist in its original form, trapped inside a primitive extraterrestrial body like a comet or undifferentiated asteroid. In practice, *presolar* (or, equivalently, *stardust*, or *circumstellar*) usually is reserved for a grain that is *demonstrably* so, that is, it has an isotopic composition in one or more element that is so far removed from the range observed in materials of known solar system origin that it must have formed before. Current astrophysical knowledge indicates that a large fraction of interstellar dust consists not of pure stardust, but of grains that have been completely reprocessed in the diffuse interstellar medium and/or molecular clouds. Such grains present in the Sun's parental cloud would likely have isotopic compositions very similar to the bulk Solar System composition and thus not be recognized as presolar grains even if found in a meteorite or cometary sample today. Thus, it must be recognized at the outset that the isotopically anomalous grains recognized as presolar stardust are not likely to be a representative sample of Galactic dust in general or of the starting dust of our planetary system. However, as pristine solid samples of stellar matter available for study in the laboratory, they provide unique astrophysical information and insights not obtainable by other

FIG. 1

(a) Scanning electron micrograph of Al_2O_3 grain 83–5, the first presolar oxide grain identified on the basis of anomalous O isotopes. The grain has been sputtered in an ion microprobe and is sitting on a mesa of the Au substrate. (b) Discovery data for 83–5. Plotted is a histogram of $\delta^{18}O$ values automatically determined for oxide grains in an acid residue of the Murchison meteorite, with outlier 83–5 indicated. Subsequent measurements also showed this grain to be highly enriched in ^{17}O and radiogenic ^{26}Mg.

means and their study is complementary to astronomical observations and astrophysical theory.

In this chapter, we define a presolar oxide grain as a dust grain containing oxygen, but not silicon, as a major element, whose composition in at least one isotopic ratio is clearly outside the range of Solar System materials. The latter definition is complicated by the fact that the known O-isotopic range of the Solar System has expanded since the original identification of presolar grains. The vast majority of presolar oxide grains are identified as such by having anomalous $^{17}O/^{16}O$ and/or $^{18}O/^{16}O$ ratios; the O isotope data for such O-anomalous grains (oxides and silicates) are plotted in Fig. 2 and span many orders of magnitude in both ratios. The second panel zooms in on the data near the composition of the Solar System. At the time presolar oxides were first being discovered, the bulk O isotopic composition of the Sun was believed to be close to that of the Earth with only the CAIs showing a 5% enrichment in ^{16}O. More recently, data from NASA's Genesis mission was used to infer that the Sun itself is ^{16}O-rich (McKeegan et al., 2011), relative to the Earth. Moreover, Sakamoto et al. (2007) discovered an unusual material, since named "cosmic symplectite" or COS, in the ungrouped carbonaceous chondrite Acfer 094 with a 20% depletion in ^{16}O, relative to the Earth. This material—a fine-grained mixture of iron sulfide and iron oxide—most likely formed by interaction of a ^{16}O-poor H_2O reservoir in the protoplanetary disk with preexisting metal and sulfide grains. The same isotopic composition has been subsequently found in silicate material within an IDP of likely cometary origin. Therefore, the range of Solar System O isotopes is now known to extend to ^{17}O- and ^{18}O-rich compositions, as indicated by the shaded region in Fig. 2b (Online Supplementary Data 1 and 2 in the online version at https://doi.org/10.1016/B978-0-12-821830-3.00010-3). Some 1%–2% of reported "presolar" oxides and silicates have isotopic compositions in this range and their identification as demonstrably presolar stardust grains must now be taken as ambiguous. It may well be that the process(es) responsible for producing this isotope signature in the Solar System would not transmit it into a refractory oxide like Al_2O_3 and all alumina grains with O isotopes in this range are indeed stardust, but this subject deserves much further scrutiny. In any case, it is safe to conclude that essentially all grains with O isotopic ratios that differ from the Earth by >20% are indeed presolar stardust grains.

In addition to presolar grains with substantial O isotope anomalies, a few oxide grains with isotopically normal O but highly unusual Mg isotopes have also been identified (Choi et al., 1998). The origins of these are ambiguous and they will not be discussed further here. More recently, very small (<100 nm) oxide grains with highly unusual Cr and Ti isotopic compositions have been identified in residues of the Orgueil meteorite (Dauphas et al., 2010; Qin et al., 2011; Nittler et al., 2018). These appear to have fundamentally different origins than the vast majority of the O-anomalous grains shown in Fig. 2, though it has not yet been possible to accurately determine their O isotope ratios. These grains will be discussed separately.

We note that just as our knowledge of the O isotopic composition of the Solar System has evolved since the early 1990s, so has the technology used to isotopi-

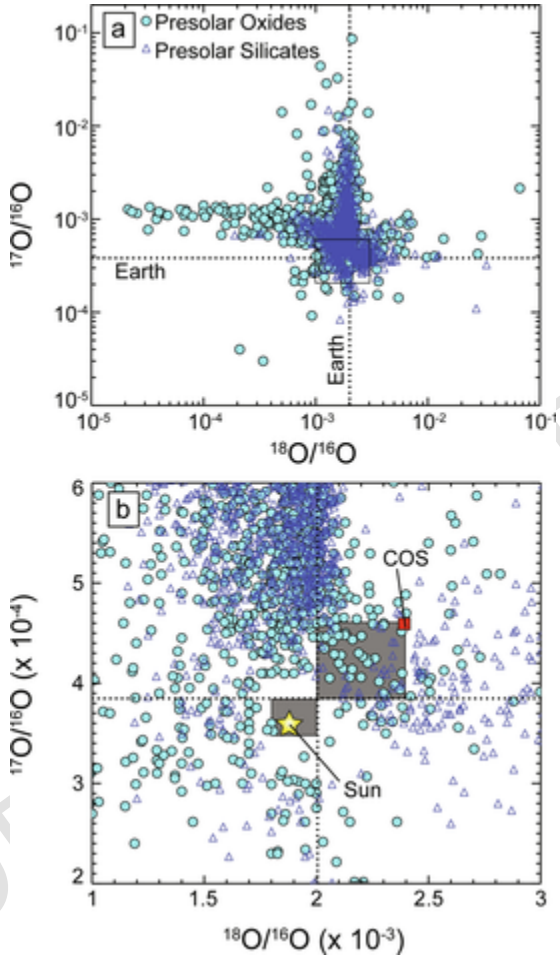

*- Data are taken from a large number of sources (*Online Supplementary Data 1 and 2*), including Nittler, L., Alexander, C.M.O'D., Gao, X., Walker, R.M., Zinner, E., 1994. Interstellar oxide grains from the Tieschitz ordinary chondrite. Nature 370, 443–446; Nittler, L.R., Alexander, C.M.O'D., Gao, X., Walker, R.M., Zinner, E., 1997. Stellar sapphires: the properties and origins of presolar Al2O3 in meteorites. Astrophys. J. 483, 475–495; Nittler, L.R., Alexander, C.M.O'D., Gallino, R., Hoppe, P., Nguyen, A., Stadermann, F., Zinner, E.K., 2008. Aluminum-, calcium- and titanium-rich oxide stardust in ordinary chondrite meteorites. Astrophys. J. 682, 1450–1478; Nittler, L.R., Wang, J., Alexander, C.M.O'D., 2012. Confirmation of extreme 54Cr enrichments in Orgueil nano-oxides and correlated O-isotope measurements. Lunar Planet. Sci. 43, abstract #2442; Nguyen, A., Zinner, E., Lewis, R.S., 2003. Identification of small presolar spinel and corundum grains by isotopic raster imaging. Pub. Astron. Soc. Aust. 20, 382–388; Nguyen, A.N., Nittler, L.R., Stadermann, F.J., Stroud, R.M., Alexander, C.M.O'D., 2010. Coordinated analyses of presolar grains in the Allan Hills 77307 and queen Elizabeth range 99177 meteorites. Astrophys. J. 719, 166–189; Qin, L., Nittler, L.R., Alexander, C.M.O'D., Wang, J., Stadermann, F.J., Carlson, R.W., 2011. Extreme 54Cr-rich nano-oxides in the CI chondrite Orgueil—implication for a late supernova injection into the solar system. Geochim. Cosmochim. Acta 75, 629–644; Haenecour et al., 2018; Barosch, J., Nittler, L.R., Wang, J., Dobrică, E., Brearley, A.J., Hezel, D.C., Alexander, C.M.O'D., 2022a. Presolar O- and C-anomalous grains in unequilibrated ordinary chondrite matrices. Geochim. Cosmochim. Acta 335, 169–182; Barosch, J., Nittler, L.R., Wang, J., Alexander, C.M.O'D., De Gregorio, B.T., Engrand, C., Kebukawa, Y., Nagashima, K., Stroud, R.M., Yabuta, H., Abe, Y., Aléon, J., Amari, S.,*

- Amelin, Y., Bajo, K.-i., Bejach, L., Bizzarro, M., Bonal, L., Bouvier, A., Carlson, R.W., Chaussidon, M., Choi, B.-G., Cody, G.D., Dartois, E., Dauphas, N., Davis, A.M., Dazzi, A., Deniset-Besseau, A., Di Rocco, T., Duprat, J., Fujiya, W., Fukai, R., Gautam, I., Haba, M.K., Hashiguchi, M., Hibiya, Y., Hidaka, H., Homma, H., Hoppe, P., Huss, G.R., Ichida, K., Iizuka, T., Ireland, T.R., Ishikawa, A., Ito, M., Itoh, S., Kamide, K., Kawasaki, N., Kilcoyne, D., Kita, N.T., Kitajima, K., Kleine, T., Komatani, S., Komatsu, M., Krot, A.N., Liu, M.-C., Martins, Z., Masuda, Y., Mathurin, J., McKeegan, K.D., Montagnac, G., Morita, M., Mostefaoui, S., Motomura, K., Moynier, F., Nakai, I., Nguyen, A.N., Ohigashi, T., Okumura, T., Onose, M., Pack, A., Park, C., Piani, L., Qin, L., Quirico, E., Remusat, L., Russell, S.S., Sakamoto, N., Sandford, S.A., Schönbächler, M., Shigenaka, M., Suga, H., Tafla, L., Takahashi, Y., Takeichi, Y., Tamenori, Y., Tang, H., Terada, K., Terada, Y., Usui, T., Verdier-Paoletti, M., Wada, S., Wadhwa, M., Wakabayashi, D., Walker, R.J., Yamashita, K., Yamashita, S., Yin, Q.-Z., Yokoyama, T., Yoneda, S., Young, E.D., Yui, H., Zhang, A.-C., Abe, M., Miyazaki, A., Nakato, A., Nakazawa, S., Nishimura, M., Okada, T., Saiki, T., Tanaka, S., Terui, F., Tsuda, Y., Watanabe, S.-i., Yada, T., Yogata, K., Yoshikawa, M., Nakamura, T., Naraoka, H., Noguchi, T., Okazaki, R., Sakamoto, K., Tachibana, S., Yurimoto, H., 2022b. Presolar stardust in asteroid Ryugu. Astrophys. J. 935, L3, and many others.

cally analyze presolar grains and every method has introduced its own biases. All early studies of presolar oxides were based around Cameca ims-3f ion probes. Such instruments were well suited to measurements of single grains larger than about 1 μm, so early studies also targeted meteoritic acid residues sorted into grains of this size. While the automated ims-3f-based ion imaging searches for presolar oxide grains described in Section 1 were successful (Nittler et al., 1994, 1997), they were based on locating grains with anomalous $^{18}O/^{16}O$ ratios and thus were biased against grains with normal ^{18}O but anomalous $^{17}O/^{16}O$ ratios, many of which are now known to exist (e.g., they plot along the vertical dashed line in Fig. 2). The development of fully automated single-grain measurements on the ims-6f ion probe (Nittler and Alexander, 2003; Nittler et al., 2008) provided a new method for efficiently identifying presolar oxides without this bias, but was still mainly limited to grains larger than ~1 μm in diameter. The development of the NanoSIMS ion probe with its high sensitivity and typical spatial resolution of <100 nm allowed submicron presolar grains of all phases, including silicates and oxides, to be identified and measured. NanoSIMS-based raster ion imaging of crowded samples (e.g., IDP or meteoritic thin sections or dispersed and size-sorted meteoritic matrix materials deposited in thick layers on SIMS substrates) was soon found to be an efficient way to identify rare presolar oxide and silicate grains (Messenger et al., 2003; Nguyen et al., 2003). However, compared to single-grain measurements of grains dispersed and well separated on substrates, NanoSIMS imaging data is much more strongly affected by the possible inclusion of contaminating signals. Even when focused on a small spot, the NanoSIMS primary ion beam has Gaussian-like tails that result in "dilution" of the desired measured signals with atoms sputtered from surrounding materials. This dilution has two undesirable results: (1) Even when detected, isotopic anomalies can only be considered lower limits on a grain's true composition, which complicates quantitative comparison with predictions of astrophysical models, for instance. Modeling is sometimes used to estimate the degree of dilution and in some cases to correct measured isotope ratios (Nguyen et al., 2007; Qin et al., 2011; Hoppe et al., 2018). However, Barosch et al. (2022a) recently argued that such efforts are highly inaccurate due to degeneracy between the degree of anomaly and grain size. (2) Detection limits for presolar grains decline precipitously with decreasing grain size such that grains near or below the primary ion beam size are likely to not be identified, depending to a large extent on how anomalous they are

FIG. 2

O isotopic ratios in ~1650 presolar oxide and ~1700 presolar silicate grains, plotted with (a) logarithmic axes and (b) linear axes with reduced ranges (location of panel b is indicated by box on panel a). The *dotted lines* indicate the terrestrial O isotope ratios: $^{17}O/^{16}O = 3.829 \times 10^{-4}$, $^{18}O/^{16}O = 0.002$. *Shaded regions* on (b) indicate the range of O isotope ratios observed in materials of known Solar System origin, defined by end-members of the Sun (McKeegan et al., 2011) and cosmic symplectite (COS; Sakamoto et al., 2007). A few percent of reported presolar grains have compositions that overlap the Solar System and thus may not in fact have a presolar origin.

(it is easier to detect a grain whose $^{17}O/^{16}O$ ratio is 20× that of the Earth than one with a ratio 1.5 times higher). Thus, even if we define presolar grains as those with demonstrably anomalous isotope compositions, datasets will usually have intrinsic biases toward larger and more anomalous grains and estimates of presolar grain abundances in different planetary materials are, by definition, lower limits. One further complication is inconsistency in the literature in how anomalous a grain must be to be considered presolar. In the early days, a significance level of 2 or 3 sigma for a measured isotopic anomaly was commonly taken as "good enough" to consider a grain truly anomalous, whereas recent studies have been much more conservative (Hoppe et al., 2015; Barosch et al., 2022a). The changes in analysis technology with time and the various biases introduced as a consequence make it challenging at times to fully consider the published datasets as a whole, for example, to compare presolar oxides, many of which were identified by single-grain analysis, to presolar silicates, all of which were found by raster ion imaging and thus subject to isotope dilution.

3 Types and sizes of presolar oxide grains

As mentioned in Section 1, the first presolar oxide phase to be identified in meteoritic samples was alumina (Al_2O_3), followed by spinel ($MgAl_2O_4$) and hibonite ($CaAl_{12}O_{19}$). Since then, as summarized in Table 1 and illustrated in Fig. 3a, at least four additional presolar oxide phases have been identified, as well as complex grains consisting of oxide and silicate phases intergrown or associated with each other. We note that in most cases phase identification has been made on the basis of major-elemental chemical data obtained by (in increasing order of accuracy) secondary ion mass spectrometry (SIMS), energy-dispersive X-ray analysis (EDS) in the scanning electron microscope (SEM), or Auger electron spectroscopy (AES),

TABLE 1 Presolar oxide phases.

Phase[a]	Number[b]
Al_2O_3	711
Spinel ($MgAl_2O_4$)	415
Hibonite ($CaAl_{12}O_{19}$)	32
Cr-Spinel $(Mg,Fe)Cr_2O_4$	7
Fe oxides	6
^{54}Cr-rich	30
U[c]	480

[a] *Estimated from SEM-EDS or SIMS elemental abundances. See* Tables 4–6 *for grains with more precise phase identifications.*
[b] *Number reported in literature.*
[c] *Unknown or unspecified.*

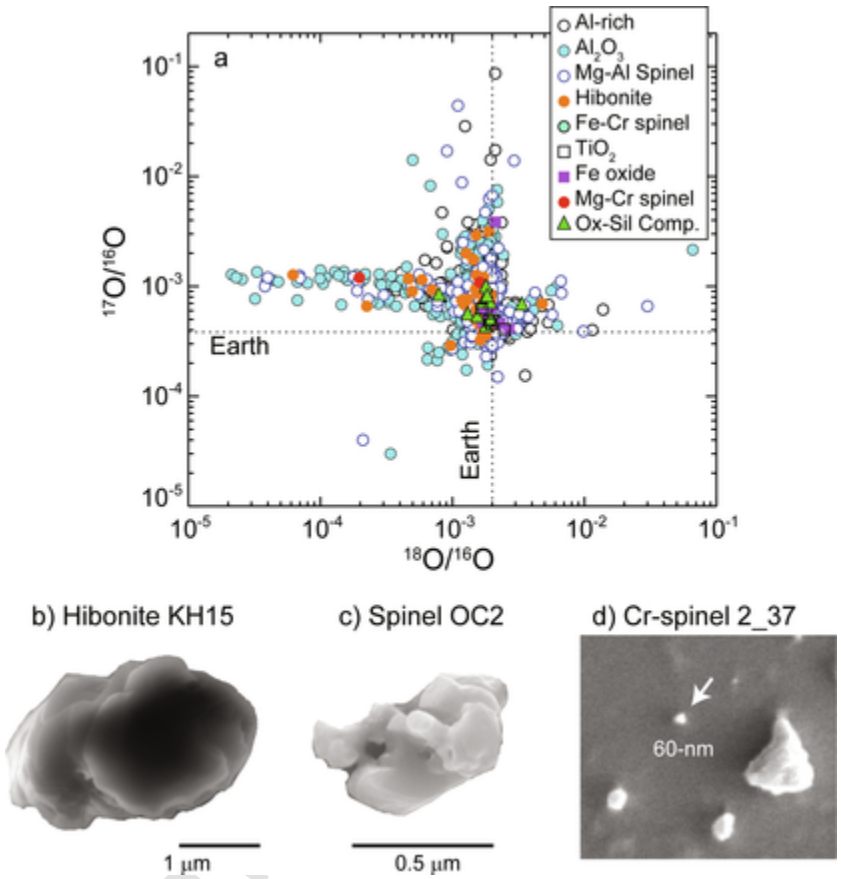

FIG. 3

(a) O 3-isotope plot showing different oxide phases. Bottom: Scanning electron microscope images of (b) 3-µm hibonite KH15 (Nittler et al., 2008; Zega et al., 2011), (c) ~0.5 µm spinel grain OC2 (Lugaro et al., 2007), and (d) a 60-nm ^{54}Cr-rich oxide grain (Nittler et al., 2018).

each of which has its limitations as to detection limits, accuracy, etc. For example, hibonite has a similar chemical composition to Al_2O_3, except for a small amount (~6 wt%) of calcium, so the SEM-EDS spectrum of a small hibonite grain may not show the Ca peak, depending on instrument conditions, resulting in misidentification as Al_2O_3. Roughly one-fourth of the presolar oxides reported to date are simply described as Al-rich, usually based on NanoSIMS data, and indicating that they could be Al_2O_3, spinel, hibonite, or another phase. Some are reported only as oxides, based on a lack of Si signals in the NanoSIMS measurements that identified the grains as presolar. The most accurate phase identifications are made through transmission electron microscopy (TEM), which can provide both nm-scale mi-

crostructural information and chemical composition. Although TEM has only been applied to a relatively small number of presolar oxide grains, such measurements have provided important information about several major presolar oxide types, as detailed in Section 6.

Grain sizes have not been explicitly provided for all presolar oxide grains in the literature, but reported diameters range from smaller than 100 nm for the most ^{54}Cr-rich nano-spinels to several micrometers for many Al-rich grains (e.g., Fig. 3, bottom). As mentioned in Section 2, larger grains are especially prevalent in studies from the 1990s and early 2000s that used ims-3f and ims-6f ion microprobes. However, presolar oxides larger than 1 μm have continued to be reported in in situ NanoSIMS searches of meteorites (Leitner et al., 2018; Nittler et al., 2021). In the case of the ^{54}Cr-rich grains, there is a clear inverse dependence between the degree of isotopic anomaly and size (Nittler et al., 2018). In contrast, for O-anomalous oxides, there is no clear evidence for any relationship between grain size and isotopic composition (Fig. 4). The broadest range of both $^{17}O/^{16}O$ and $^{18}O/^{16}O$ ratios is seen for grains of a few hundred nm in diameter, but this is also the most typical grain

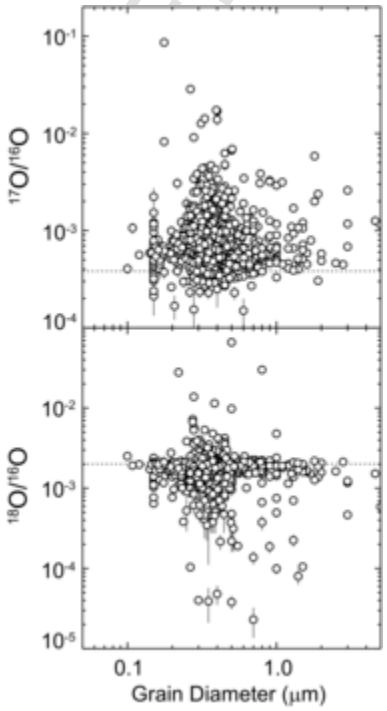

FIG. 4

The O-isotopic ratios of presolar oxide grains plotted against their diameters. The *horizontal dashed lines* indicate the terrestrial isotopic ratios.

size in the database. Note that the clear vertical concentrations of grains at ~150-nm diameter are due to spinel and Al_2O_3 grains identified in the "CF" acid residue of the Murray CM chondrite (Nguyen et al., 2003; Zinner et al., 2003; Gyngard et al., 2010b); individual grain sizes were not reported for these grains, so they were assigned the mean size of the residue. In actual fact, these probably range from ~100 to 200 nm in diameter. Although one might expect that the isotopic dilution that affects grains measured by raster ion imaging (Section 2) would lead to less anomalous compositions for such grains on average, the situation is more complicated. Such dilution is in fact just as likely to lead more to non-detection of the smallest grains, except those with more extreme anomalies; therefore, the oxide grain with the highest $^{17}O/^{16}O$ ratio (~0.1) is also one of the smallest identified O-anomalous grains, <200 nm in diameter.

4 Isotopic characteristics

4.1 O-isotope groups

Although the first few identified presolar oxide grains (Nittler et al., 1993; Huss et al., 1994) had roughly similar isotopic compositions, by the time a couple of dozen had been identified, it was clear that they fall in different parts of the oxygen 3-isotope diagram (e.g., Fig. 2), likely reflecting different stellar sources and/or processes. Nittler et al. (1994, 1997) divided the data into four isotopic groups, a system that is still in wide use today, for both presolar oxides and silicates, although definitions have been refined over time and some grains with compositions outside the main groups gave been identified. The Group definitions we use here differ somewhat from those in the literature and are summarized in Table 2 and Fig.

TABLE 2 Presolar oxide groups.

Group	Definition	Percentage[a]
1	$3.38\times10^{-4}<{}^{17}O/^{16}O<5\times10^{-3}$ $1\times10^{-3}<{}^{18}O/^{16}O<\sim0.002$	74
2	$^{17}O/^{16}O>\times10^{-4}$ $^{18}O/^{16}O<1\times10^{-3}$	9
3	$1\times10^{-4}<{}^{17}O/^{16}O<3.38\times10^{-4}$ $^{17}O/^{18}O>0.19$	5
3 ^{18}O-rich	$1\times10^{-4}<{}^{17}O/^{16}O<3.38\times10^{-4}$ $^{17}O/^{18}O<0.19$	1.7
4	$^{18}O/^{16}O>0.002$ $\delta^{17}O<5.5\times\delta^{18}O$	9
1× ^{16}O-rich	$^{17}O/^{16}O>5\times10^{-3}$ $^{17}O/^{16}O<1\times10^{-4}$ $^{18}O/^{16}O<1\times10^{-3}$	0.01 0.001

See text for details.

[a] *Based on 1650 total reported grains.*

5. It is important to note that this classification system, while useful for aiding in discussions, is to a large extent arbitrary. The O isotopic compositions of grains within most groups span wide ranges and the Groups are not generally cleanly sep-

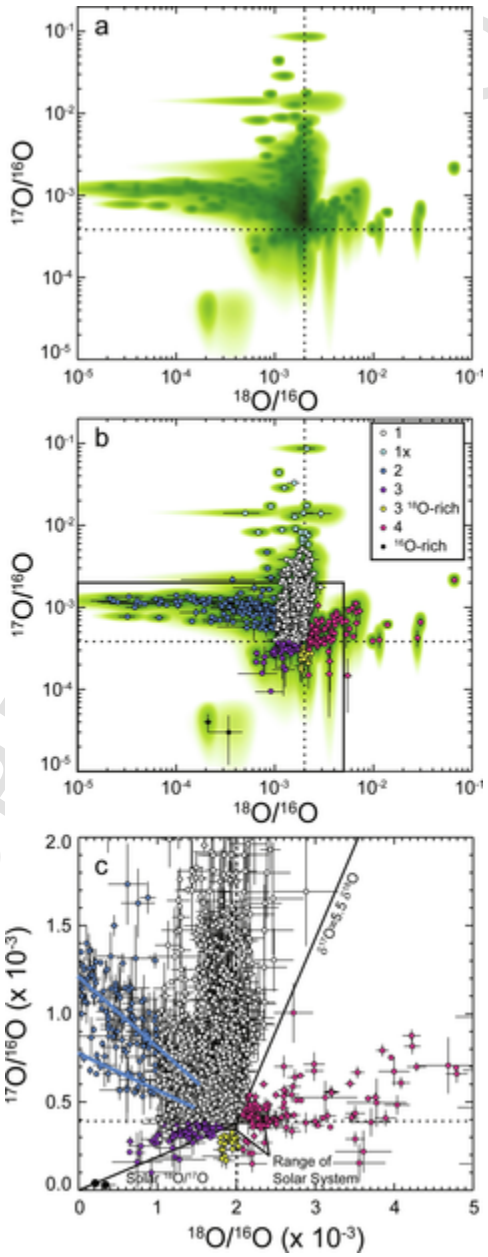

arated from each other. Moreover, although it is tempting to assume that each Group represents a single type of stellar source (evolved low-mass stars vs Type II supernovae, for instance), multielemental isotopic data for many grains as well as astrophysical considerations indicate it is not so simple: most Groups may well contain grains from more than one type of stellar source and the same type of source can provide grains with compositions in different Groups. In general, the groupings in O-isotopic space reflect a combination of starting compositions of stars, specific stellar nuclear and mixing processes that affect O isotopes, and the different sources where such processes occur. As explained below in Section 5, the main nucleosynthetic processes that affect O isotopes—H- and He-burning—occur in essentially all stars (see also Chapters 7–9). A major challenge of presolar grain research is to work backward from measured compositions, while using the tools of astrophysics, to work out which types of stars produced which specific stardust grains and, hopefully, then use the grain data to learn new things about the parent stars. Classifying the grains into Groups is a useful first step in this process. Here we explain the Group definitions as used in this chapter.

Fig. 5 includes data for about 1650 individual presolar oxide grains and with large numbers of overlapping data points, it can be hard to discern the density of points on scatter plots. To better visualize the distribution of presolar oxides in O isotope space, Fig. 5a thus shows a probability distribution derived from the grain data, generated by summing two-dimensional Gaussian distributions according to the measurement errors for each grain. In Fig. 5b, the individual grain data are plotted over the probability distribution and in Fig. 5c, the data are shown with linear axes over a smaller plotting range.

The overwhelming majority of presolar O-anomalous grains plot in the upper left quadrant of Fig. 5 (enriched in ^{17}O and depleted in ^{18}O, relative to the terrestrial composition). These grains have long been divided into two Groups, 1 and 2 (Nittler et al., 1994), and the existence of at least two distinct trends, which overlap and merge close to Solar, is clearly seen in the probability distribution (Fig. 5a). Nittler et al. (1997) originally used a threshold value of $^{18}O/^{16}O = 8 \times 10^{-4}$ to separate Group 1 and 2 grains. Based on the probability density plot, it is clear that the Group 1 and 2 trends merge as both approach the terrestrial composition, so any single ratio cutoff is arbitrary. Nevertheless, here we define Group 2 grains as those having $^{18}O/^{16}O < 1 \times 10^{-3}$, with the recognition that grains with $^{17}O/^{16}O < 1 \times 10^{-3}$ and $^{18}O/^{16}O > 1 \times 10^{-3}$ lie in the overlap region between the two Groups. Note also that most grains in this quadrant of the plot have $^{17}O/^{16}O$ ratios lower than a few

FIG. 5

(a) The O-isotopic distribution of presolar oxide grains displayed as a false-color probability density plot (darker equals higher density). (b) Oxide grain data overlain on probability density map, color-coded to indicated group definitions. (c) Presolar oxide O-isotopic data displayed with linear axes and a more limited range than (a and b), indicated by *solid lines* on (B). The *dotted lines* indicate the terrestrial isotopic ratios.

times 10^{-3}. Nittler et al. (2008) argued that grains with $^{17}O/^{16}O$ ratios higher than this may have origins distinct from the other grains, and these have been called variously "^{17}O-rich," "extreme Group 1," or Group "1x" grains. We adopt the latter nomenclature and use a threshold value of $^{17}O/^{16}O = 5 \times 10^{-3}$ to distinguish Group 1x grains from Group 1 and 2 grains; this value is based on expectations for low-mass asymptotic giant branch (AGB) stars, the likely sources of many Group 1 grains, as discussed further in Section 5. With these definitions, Group 1 grains make up 75% and Group 2 8.5% of the reported presolar oxide data. Note that isotope dilution for grains measured by in situ ion imaging has undoubtedly led to an overestimate of $^{18}O/^{16}O$ ratios in some Group 1 and 2 grains and the true fraction of Group 2 grains is probably higher (and Group 1 slightly lower) as a result; this is a more significant problem for presolar silicates (Chapter 6).

Despite the overlap with Group 1 close to normal composition, the defining characteristic of Group 2 grains is their substantial ^{18}O depletions, with $^{18}O/^{16}O$ ratios essentially ranging all the way to zero, coupled with ^{17}O enrichments. Most, but not all, of the defined Group 2 grains define two linear trends (*blue lines*) on the O-isotope plot, corresponding roughly to mixing lines between end-members with ($^{17}O/^{16}O = 8 \times 10^{-4}$, $^{18}O/^{16}O = 0$) and ($^{17}O/^{16}O = 1.2 \times 10^{-3}$, $^{18}O/^{16}O = 0$) and a more solar-like composition. A small number of Group 2 grains range to much higher $^{17}O/^{16}O$ ratios, however.

Group 3 grains were originally defined as having $^{17}O/^{16}O$ ratios equal to or lower than the terrestrial value and most of the originally identified Group 3 grains had ^{18}O depletions as well, with $^{17}O/^{18}O$ higher than the Solar System value of 0.19. There is strong evidence that most of these are related to Group 1 grains and represent a population of grains formed in low-mass, low-metallicity AGB stars (Sections 5.2 and 5.4). However, as the database of known O-anomalous presolar grains has grown, it has become increasingly clear that ^{17}O-poor grains in fact plot in two distinct clusters, with one group of grains having higher (closer to normal) $^{18}O/^{16}O$ ratios (*yellow symbols* in Fig. 5). Nittler et al. (2020) suggested that these might be related to the ^{18}O-rich Group 4 grains (see below) and proposed including them in the Group 4 definition. However, at least for presolar oxides, these grains are clearly distinct from most Group 4 grains (most of which have terrestrial or higher $^{17}O/^{16}O$ ratios). Unfortunately, there is little isotope data available for elements other than O for these grains and their origins are thus still quite ambiguous. Here we consider any ^{17}O-poor grain with $^{17}O/^{18}O$ higher than or within error of the terrestrial value to be Group 3 grains (5% of total) and refer to ^{17}O-poor grains with lower $^{17}O/^{18}O$ (higher $^{18}O/^{16}O$) ratios as "^{18}O-rich Group 3" grains (1.7%).

Group 4 grains were originally defined as having enrichments in both ^{17}O and ^{18}O, relative to the Solar System (Nittler et al., 1997), but it soon became clear that there also exist ^{18}O-enriched presolar grains with terrestrial (Choi et al., 1998) or even depleted (Messenger et al., 2005) $^{17}O/^{16}O$ ratios, both types of which are now included in Group 4 (Table 2). Note that while Group 1 grains were originally defined as having terrestrial or lower $^{18}O/^{16}O$ ratios, a small fraction of grains defined as Group 1 in fact have higher than terrestrial $^{18}O/^{16}O$. This is most visible for

grains with $^{17}O/^{16}O > 6 \times 10^{-4}$ (Fig. 5c), but there is some ambiguity in distinguishing Groups 1 and 4 for grains closer to Solar in composition. Here we arbitrarily set the dividing line for ^{18}O-enriched grains such that Group 1 grains have $\delta^{17}O/\delta^{18}O > 5.5$ (Fig. 5c), where δ denotes the usual geochemical δ-value ($\delta R = (R/R_{std} - 1)\,1000$, with R_{std} being a reference ratio, in this case Earth's ocean water. Note that the region on the O 3-isotope plot where there is the most ambiguity in distinguishing Group 1 and 4 grains also corresponds to the region now known to include materials of Solar System origin (Section 2; Figs. 2b and 5c) and many of these grains may not in fact be bona fide presolar stardust grains, including some 20% of Group 4 grains.

Finally, two presolar oxide grains, one alumina and one spinel, with almost-pure-^{16}O compositions have been identified (Nittler et al., 1998; Gyngard et al., 2010b). These plot far outside the other Groups and clearly form their own, still limited, population.

4.2 Mg-Al isotopes

Mg-Al isotopic data have been reported for >200 presolar oxide grains and the data are shown in Fig. 6. The most striking feature of the $^{25}Mg/^{24}Mg$ vs $^{26}Mg/^{24}Mg$ plot (Fig. 6a) is the much larger range of $^{26}Mg/^{24}Mg$ ratios, especially for Al-rich phases, compared to $^{25}Mg/^{24}Mg$ ratios. Whereas most grains have $^{25}Mg/^{24}Mg$ ratios within a factor of 2 of the solar value of 0.1266, $^{26}Mg/^{24}Mg$ ratios range up to several 100, or greater than 2000 times the solar value of 0.13932. Such a pronounced effect in a single isotopic ratio is commonly a signature of radioactive decay and, indeed, in this case this is the telltale sign that many of the grains incorporated live ^{26}Al ($t_{½}$ = 720,000 yr) into their structures, which subsequently decayed to ^{26}Mg. One can infer the initial $^{26}Al/^{27}Al$ ratio of a grain from its Al/Mg elemental ratio and excess amount of ^{26}Mg from radioactive decay (e.g., Nittler et al., 1997). This is illustrated in Fig. 6b, which shows $^{26}Mg/^{24}Mg$ ratios plotted against $^{27}Al/^{24}Mg$ ratios for the presolar oxide grains. Solid curves indicate inferred initial $^{26}Al/^{27}Al$ ratios for given Mg-Al isotopic compositions; the grains range from containing essentially no extinct ^{26}Al to having formed with up to 10% of their Al atoms being ^{26}Al. Note that the CAIs discussed at the beginning of this chapter also show ^{26}Mg excesses attributable to ^{26}Al decay and this isotope was very likely an important heating source for the initial stages of planet formation in the Solar System. However, the maximum $^{26}Al/^{27}Al$ ratio inferred for CAIs is only about 5×10^{-5}. The much higher ratios seen in many presolar oxide grains constitute further proof that they are indeed presolar stardust that contain a record of nucleosynthesis in their parent stars.

The inferred initial $^{26}Al/^{27}Al$ ratios for the presolar alumina and hibonite grains are plotted against their $^{18}O^{16}O$ ratios in Fig. 6d. As is clear from Fig. 6a–c, many presolar spinel grains also have ^{26}Mg excesses. However, for a large fraction of these, the observed anomalies in ^{25}Mg are of comparable magnitude to those in ^{26}Mg (e.g., Fig. 6c). In such cases, it is impossible to unambiguously distinguish

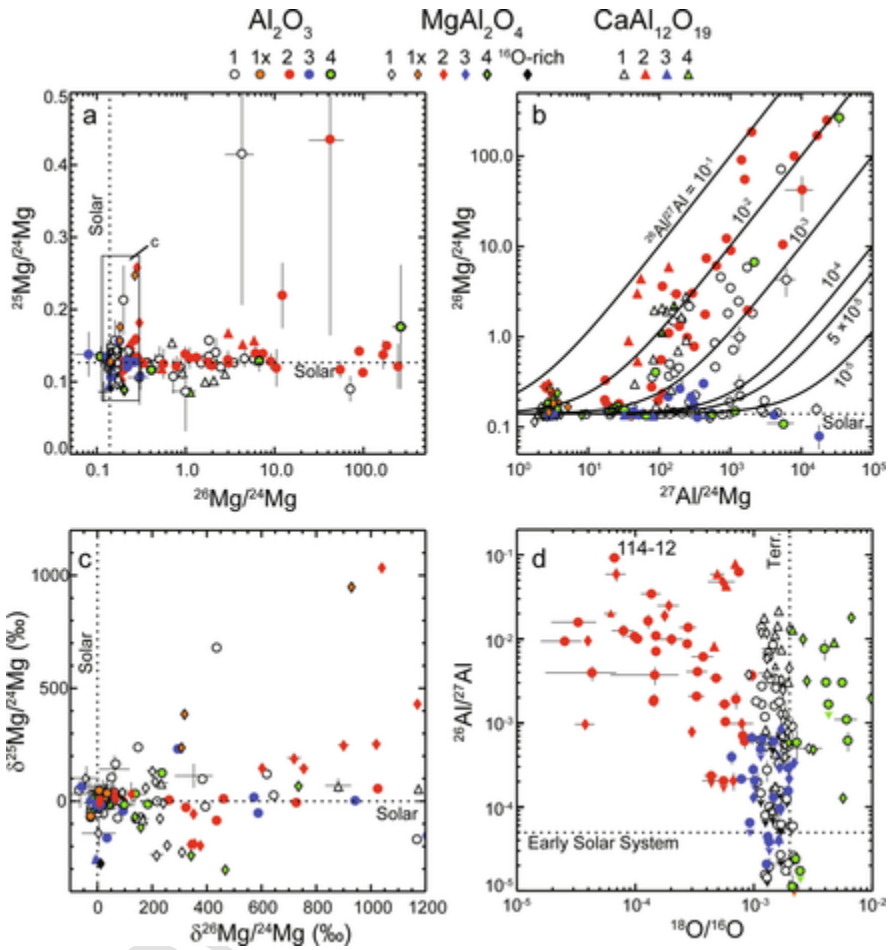

FIG. 6

Magnesium and aluminum data for presolar oxide grains. (a) $^{25}Mg/^{24}Mg$ plotted vs $^{26}Mg/^{24}Mg$ ratios. (b) $^{25}Mg/^{24}Mg$ plotted vs $^{27}Al/^{24}Mg$ ratios. *Curves* indicate isochrons for different amounts of extinct ^{26}Al. (c) Zoom in on rectangular area of panel (A). (d) Inferred initial $^{26}Al/^{27}Al$ ratios plotted vs $^{18}O/^{16}O$ ratios.

excess ^{26}Mg from ^{26}Al decay and excess ^{26}Mg from nuclear processes directly affecting Mg isotopes. We therefore do not include spinel data in Fig. 6d. However, Zinner et al. (2005) used nucleosynthetic models of AGB stars (the presumed sources of many of the presolar grains) to correct for nucleosynthetic Mg anomalies and thereby estimate the initial amounts of ^{26}Al in presolar spinels. They found a similar range of $^{26}Al/^{27}Al$ ratios to those seen for presolar alumina and hibonite. From Fig. 6d, we can see: (1) About one-third of Group 1 presolar oxide grains do

not show excess ^{26}Mg, but those that do have inferred ^{26}Al/^{27}Al ratios mainly ranging from a few times 10^{-4} to ~0.02. (2) Almost all Group 2 grains (all those with $^{18}O^{16}O < 4 \times 10^{-4}$) have evidence for extinct ^{26}Al, with ^{26}Al/^{27}Al ratios ranging from $\sim 2 \times 10^{-3}$ up to 0.1. (3) Group 3 grains generally show little evidence for extinct ^{26}Al; those with excess ^{26}Mg have relatively low ^{26}Al/^{27}Al ratios, $<10^{-3}$. (4) Almost all Group 4 grains have ^{26}Mg excesses, with inferred ^{26}Al/^{27}Al ratios similar to those of Group 1 grains.

Although decay of ^{26}Al has led to much larger apparent effects in ^{26}Mg than in ^{25}Mg for many presolar oxide grains, anomalous ^{25}Mg/^{24}Mg ratios are not unusual (Fig. 6). Grains with $>2\sigma$ anomalies in ^{25}Mg/^{24}Mg make up 50%–60% of the presolar hibonite and spinel grains that have been measured for Mg isotopes and 15% of measured Al_2O_3 grains. The much smaller fraction for Al_2O_3 reflects the lower Mg contents for this phase (e.g., Fig. 6b), compared to the others, and the consequently larger error bars on isotope measurements. Note that both enrichments and depletions in ^{25}Mg are seen mostly in the range of ±30% of Solar and there is little, if any, correlation with the grain group defined on the basis of O isotopes. For example, grains with δ^{25}Mg ~ −300 to −200‰ and δ^{26}Mg = 0 to +400‰ belong to all four groups and also include a ^{16}O-rich spinel (Fig. 6c). The highest observed δ^{25}Mg values of ~1000 are comparable to those recently seen in presolar silicates (Leitner and Hoppe, 2019; Hoppe et al., 2021), though the latter reach values as high as 2000‰ (Verdier-Paoletti et al., 2019).

4.3 K, Ca, Ti, and Fe isotopes

Hibonite contains Ca as a major element, and some presolar hibonites have been measured for their calcium (and potassium) isotopic systematics. Like ^{26}Al, ^{41}Ca is a short-lived isotope ($t_{½}$ = 100,000 yr) whose presence in the early Solar System has been inferred in CAIs by excesses in the decay product ^{41}K (Srinivasan et al., 1994; Liu et al., 2012). The first evidence for extinct ^{41}Ca in presolar grains was reported by Amari et al. (1996), who found ^{41}K excesses in a number of presolar graphite grains of probable supernova origin, with inferred ^{41}Ca/^{40}Ca ratios of order 10^{-3} to 10^{-2}, 6–7 orders of magnitude higher than the early Solar System ratio. Of 18 presolar hibonite grains measured for K-Ca, 11 showed ^{41}K excesses, with inferred ^{41}Ca/^{40}Ca ratios ranging from $\sim 10^{-5}$ to 4×10^{-4} (Choi et al., 1999; Nittler et al., 2008), substantially lower than those seen in the supernova graphite grains, but still vastly higher than the early Solar System. Moreover, 10 of the 18 measured grains showed anomalies in at least one of the other stable Ca isotope ratios (^{42}Ca/^{40}Ca, ^{43}Ca/^{40}Ca, and/or ^{44}Ca/^{40}Ca; neither ^{46}Ca/^{40}Ca nor ^{48}Ca/^{40}Ca were measured in these studies). The anomalous grains showed a diverse set of isotopic patterns, with moderate (typically 5%–10%) enrichments or depletions of the various isotopes (Nittler et al., 2008). The largest Ca isotopic anomalies reported for a presolar oxide grain are for a Group 3 hibonite, 3-55-7, with δ^{43}Ca = 270‰ and δ^{44}Ca = 460‰ (Nittler et al., 2011).

Titanium has five stable isotopes and the Ti isotopic systematics are well documented for both presolar SiC (Chapter 2; Alexander and Nittler, 1999; Gyngard et al., 2018; Nguyen et al., 2018) and graphite grains (Chapter 3; Jadhav et al., 2008). Ti is thus a potentially valuable element for linking presolar oxides and C-rich presolar grains. However, Ti-isotopic data for presolar oxides are still quite limited. This primarily reflects very low Ti contents in presolar Al_2O_3 grains. Hibonite typically contains higher amounts of Ti, but the presence of ^{48}Ca (which cannot be easily separated from ^{48}Ti in SIMS measurements) has thus far precluded its measurement. Ti-isotope patterns for 11 presolar oxides (9 Al_2O_3 and 2 TiO_2 grains) with anomalies in at least one isotope ratio are shown in Fig. 7. We have excluded two Al_2O_3 grains for which very large (~2× solar) excesses in ^{50}Ti were reported (Choi et al., 1998) as the errors were large and no similar anomalies have been seen in subsequent studies. Typically, but not exclusively, the presolar oxides show either V-shaped or inverted-V-shaped patterns with excesses or depletions, respectively, in

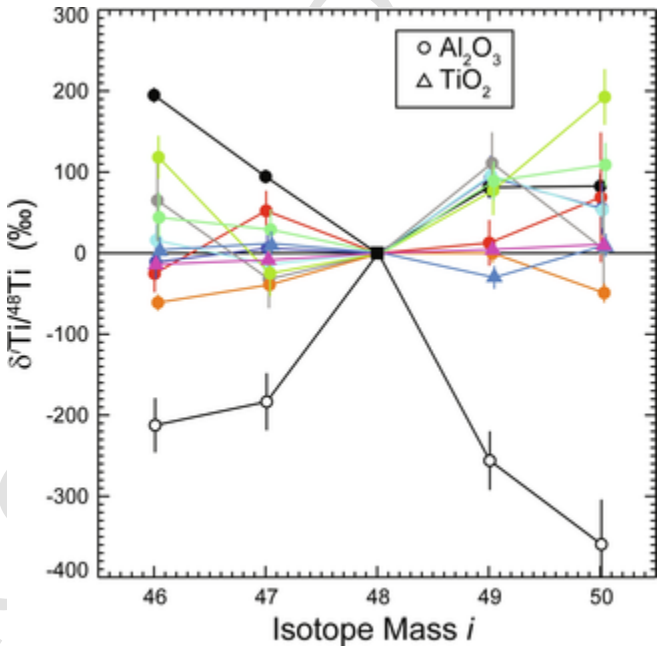

FIG. 7

Ti-isotopic ratios, expressed as δ-values, for presolar oxide grains.

- Data are from Choi, B.-G., Huss, G.R., Wasserburg, G.J., 1998a. Oxygen, magnesium, calcium, and titanium isotopes in asymptotic giant branch and supernova oxides. Meteorit. Planet Sci. Suppl. 33, A32; Hoppe, P., Nittler, L.R., Mostefaoui, S., Alexander, C.M.O'D., Marhas, K.K., 2003. A nanoSIMS study of titanium-isotopic compositions of presolar corundum grains. Lunar Planet. Sci. XXXIV, abstract 1570 (CD-ROM); Nittler, L.R., Alexander, C.M.O'D., Gallino, R., Hoppe, P., Nguyen, A., Stadermann, F., Zinner, E.K., 2008. Aluminum-, calcium- and titanium-rich oxide stardust in ordinary chondrite meteorites. Astrophys. J. 682, 1450–1478, and Hoppe (unpublished).

the rare Ti isotopes. Similar patterns are also seen for presolar SiC grains from low-mass AGB stars (Chapter 2; Hoppe et al., 1994; Alexander and Nittler, 1999). The three presolar TiO_2 grains for which Ti isotope data are available (Nittler et al., 2008) show only small anomalies.

Floss et al. (2008) and Ong and Floss (2015) reported iron isotopic data ($^{54}Fe/^{56}Fe$ and $^{57}Fe/^{56}Fe$ ratios) for some presolar O-rich grains, including five Fe-oxides. Of these, two (a Group 1 grain and a Group 4 grain) showed $>2\sigma$ anomalies in one or both Fe isotopic ratio. Both of these grains showed 10%–20% depletions of ^{54}Fe and ^{57}Fe.

4.4 ^{54}Cr-rich grains

The first hint that presolar grains enriched in ^{54}Cr might exist in meteorites was the discovery by Rotaru et al. (1992) of bulk Cr isotopic anomalies in the Orgueil CI chondrite. Their data and those of follow-up studies suggested the presence of a presolar carrier phase highly enriched in ^{54}Cr such that variations in the abundance of this carrier could lead to observable differences in bulk Cr isotopic composition (at the 10^{-4} scale) of different chondrite groups (Podosek et al., 1997; Trinquier et al., 2007). Initial searches with ims-3f ion microprobes of ~μm-sized Cr-rich grains gave ambiguous results (Nichols Jr. et al., 2000), but the development of the NanoSIMS eventually led to the discovery of tiny, highly ^{54}Cr-rich grains in acid-resistant residues of Orgueil. Even in these studies, however, the spatial resolution of the measurements (~400 nm) was coarser than the grain size (≤100 nm) of the anomalous grains, so measured compositions gave lower limits on the magnitude of the ^{54}Cr anomaly (up to 3.6× solar), making it difficult to infer the origin(s) of the grains. More recently, a new higher-resolution O^- ion source for the NanoSIMS enabled the discovery and accurate measurement of additional ^{54}Cr-rich grains (Fig. 8; Nittler et al., 2018). These authors found several grains with $^{54}Cr/^{52}Cr$ more than five times higher than solar and also exhibiting excesses at mass 50. Whether the mass-50 anomaly is carried by ^{50}Cr and/or ^{50}Ti could not be ascertained from the measurement, so the inferred $^{50}Cr/^{52}Cr$ and $^{50}Ti/^{48}Ti$ ratios were both reported for these grains (Fig. 8b and c).

5 Stellar origins of presolar oxide grains

5.1 An overview of relevant stellar processes and sites

In order to evaluate different stellar sources as potential progenitors of the observed presolar oxide grains, we briefly introduce here some concepts regarding stellar evolution and nucleosynthesis directly relevant to the interpretation of presolar oxide grains. These topics are covered in more detail in Part 2 of this book.

Stellar evolution basically describes the drawn-out battle that stars wage against collapse under their own weight. As gravity compresses stellar matter, it heats up, eventually reaching temperatures high enough that nuclei can overcome their mu-

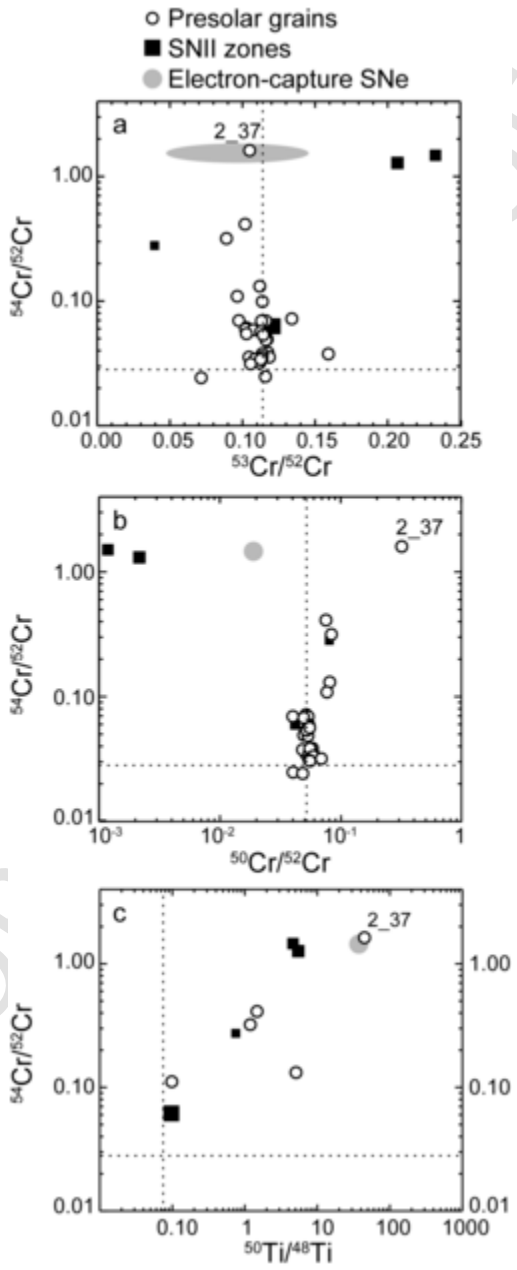

tual coulomb repulsion and undergo nuclear fusion. As long as fusion reactions are exothermic, the energy released can hydrodynamically support the star against further collapse. Once a nuclear fuel is exhausted, the stellar core can again start to collapse until heating ignites a new fuel or, if conditions are right, can be stabilized against further collapse by a quantum mechanical effect known as degeneracy pressure. Of key importance here are (1) at the temperatures and pressures experienced by stellar matter, large numbers of nuclear reactions can occur, not just those responsible for gravity-fighting energy generation, and these can lead to very large changes in isotopic ratios and (2) material that is processed by nuclear reactions may eventually be transported to exterior regions of the star via mixing, mass loss, and/or explosions, where cooling may lead to dust condensation, i.e., formation of presolar grains bearing isotopic compositions diagnostic of the nuclear processing.

Hydrogen is the most abundant element in the universe, and H-burning is the dominant nuclear process that powers stars through much of their lifetimes. In H-burning, various reactions lead to the net conversion of four protons into an α-particle (^{4}He nucleus). In low-mass stars like the Sun H-burning is dominated by the "proton-proton chain" series of reactions in which protons are built up into intermediate species (e.g., ^{3}He) before finally producing an α-particle. However, in more massive stars (>1.5$M_\odot$), if there is any C, N, and O present, a series of catalytic reactions involving the isotopes of these elements, the "CNO-cycles," dominates H-burning. The net result of the CNO-cycles is still to convert four protons into an α, but the reactions also rearrange the CNO isotopes, resulting in enrichment of ^{13}C, ^{14}N, and ^{17}O and destruction of ^{18}O and ^{15}N. Therefore, a side effect of H-burning is to lead to higher ^{17}O/^{16}O and lower ^{18}O/^{16}O ratios, i.e., the diagnostic signature of a majority of presolar oxide grains (Groups 1, 1x, and 2; Figs. 2–5). The specific isotopic ratios expected for a given star depend on a large number of factors, including the temperature and duration of burning, mixing processes, etc. At sufficiently high temperatures, additional reaction cycles can also operate during H-burning. Of the highest relevance here is the Mg-Al cycle in which proton captures can produce ^{26}Al and cause production and/or destruction of the stable Mg isotopes, depending on temperature.

Helium burning occurs following the exhaustion of H fuel in the cores of most stars and primarily serves to convert ^{4}He into ^{12}C and ^{16}O. However, as with H-burning, there are many nuclear consequences of He-burning for other elements and isotopes as well. Alpha-particle captures on ^{14}N, the main product of CNO-cycle H-burning (aside from ^{4}He), are the main nucleosynthetic source of ^{18}O via: ^{14}N(α,γ)^{18}F(e$^+\nu$)^{18}O.[a] The minor Mg isotopes, ^{25}Mg and ^{26}Mg, are produced by reactions of ^{22}Ne isotopes and α-particles, i.e., ^{22}Ne(α,n)^{25}Mg and ^{22}Ne(α,γ)^{26}Mg, where the ^{22}Ne is produced by α captures on ^{18}O. Moreover, the neutrons released

[a] Here we use a common shorthand to denote nuclear reactions, e.g., ^{14}N(α,γ)^{18}F is another way of writing ^{14}N+$\alpha\rightarrow{}^{18}$F+γ.

by the first reaction may also be captured by surrounding nuclei to produce new nuclei; of relevance here, neutron captures during He-burning can produce ^{41}Ca, ^{42}Ca, and ^{43}Ca, from ^{40}Ca, and can also enhance the minor isotopes of Ti.

Now that we have introduced H- and He-burning and their effects on the elements measured in presolar oxide grains, we turn to specific types of stellar sources where these processes occur and which therefore may be considered potential sources of the presolar oxides. Stars below about 8 times the mass of the Sun, termed low- and intermediate-mass stars, or LIMS, undergo both core H- and He-burning before ending their lives as cooling white dwarfs, stable against collapse due to electron degeneracy (Chapter 7). Following core H-burning (when the star is on the "main sequence"), a LIMS expands and becomes brighter due to shell H-burning—a red giant. At this stage, a deep mixing episode occurs, the "first dredge-up" (FDUP), in which some of the ashes of H-burning are mixed into the large convective envelope of the red giant, changing its chemical composition (for example, increasing the $^{17}O/^{16}O$ and $^{14}N/^{15}N$ ratios).

The predicted surface O isotope ratios following the FDUP (FDUP) from four different studies are shown in Fig. 9 for red giants of solar composition and masses of 1–5$M_\odot$. All models indicate that the post-FDUP $^{17}O/^{16}O$ ratio increases rapidly with stellar mass up to ~2.3$M_\odot$ and then decreases again. The precise ratio predicted for a given stellar mass depends on both the stellar model and the input nuclear physics used (e.g., reaction rates for important reactions in the CNO-cycles). The Straniero et al. (2017) model was calculated with the most recent $^{17}O(p,\alpha)^{14}N$ reaction rate and agrees well with the much older Boothroyd and Sackmann (1999) model used in many previous studies of presolar oxide grains (Nittler, 2009). However, due to the diversity in predictions reflected in Fig. 9a, we take the maximum predicted value of $^{17}O/^{16}O \approx 5 \times 10^{-3}$ from Lebzelter et al. (2015) as the value above which an origin in a low-mass AGB star is unlikely (e.g., the separation threshold between Group 1 and 1x grains, as discussed above). It has been long known (e.g., Harris and Lambert, 1984b; Dearborn, 1992) that the effect of FDUP on $^{18}O/^{16}O$ is much smaller than that on $^{17}O/^{16}O$. Mixing of partially H-burnt material lowers the envelope $^{18}O/^{16}O$ ratio by tens of %, with more recent studies favoring a maximum depletion of ~30% (Fig. 9b).

Following core He-burning, the star becomes still brighter and enters the thermally pulsing asymptotic giant branch (TP-AGB) phase. TP-AGB stars consist of an electron-degenerate core made of C and O (or O, Mg, and Ne for the most massive AGB stars, which experience partial core C-burning) surrounded by thin shells

FIG. 8

Cr- and Ti-isotopic data for small presolar oxide grains from the Orgueil meteorite with Cr anomalies (Dauphas et al., 2010; Qin et al., 2011; Nittler et al., 2018). SNII zones are calculated compositions of a 15$M_\odot$ supernova from Rauscher et al. (2002); electron capture supernova predictions are from Jones et al. (2019). The *dotted lines* indicate the terrestrial isotopic ratios.

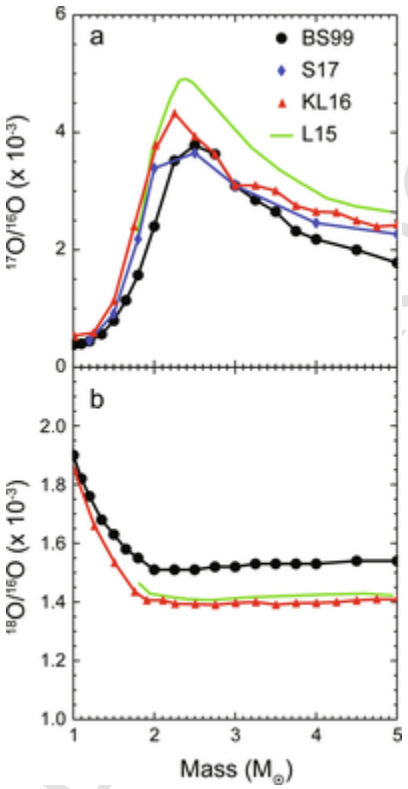

FIG. 9

Predictions of the effects of the first dredge-up on surface O-isotopic ratios of *red giant stars* of different mass.

- Data are taken from: BS99: Boothroyd, A.I., Sackmann, I.-J., 1999. The CNO-isotopes: deep circulation in red giants and first and second dredge-up. Astrophys. J. 510, 232–250; S17: Straniero, O., Bruno, C.G., Aliotta, M., Best, A., Boeltzig, A., Bemmerer, D., Broggini, C., Caciolli, A., Cavanna, F., Ciani, G.F., Corvisiero, P., Cristallo, S., Davinson, T., Depalo, R., Di Leva, A., Elekes, Z., Ferraro, F., Formicola, A., Fülöp, Z., Gervino, G., Guglielmetti, A., Gustavino, C., Gyürky, G., Imbriani, G., Junker, M., Menegazzo, R., Mossa, V., Pantaleo, F.R., Piatti, D., Piersanti, L., Prati, P., Samorjai, E., Strieder, F., Szücs, T., Takács, M.P., and Trezzi, D., 2017. The impact of the revised 17O(p, α)14N reaction rate on 17O stellar abundances and yields. Astron. Astrophys. 598, A128; KL16: Karakas, A.I., Lugaro, M., 2016. Stellar yields from metal-rich asymptotic giant branch models. Astrophys. J. 825, 26; L15: Lebzelter, T., Straniero, O., Hinkle, K.H., Nowotny, W., Aringer, B., 2015. Oxygen isotopic ratios in intermediate-mass red giants. Astron. Astrophys. 578, A33.

of He and H and a large convective envelope. The He- and H-shells alternately ignite and power the star in a series of thermal pulses. In between the pulses, material gets mixed from the region between the shells into the envelope, further changing the composition, a process known as the “third dredge-up” (a second dredge-up oc-

curs early in the AGB phase for more massive AGB stars). The most dramatic effect of the third dredge-up is to gradually increase the envelope abundance of ^{12}C, produced by shell He-burning, eventually increasing the envelope C/O ratio above unity, which has dramatic consequences for the chemistry of dust grains condensing in AGB star outflows. When C < O, O-rich phases like oxides and silicates are predicted and observed to condense, whereas once C exceeds O, a C-rich chemistry occurs producing organic molecules and refractory phases like graphite and SiC. Besides ^{12}C, however, a multitude of other isotopes affected by shell H- and He-burning are also mixed into the envelope, including radioactive nuclei like ^{26}Al and ^{41}Ca, Mg, Ca, and Ti isotopes affected by He-burning, and heavy elements produced by the so-called *s*-process, or slow neutron capture. Dust condensation in the outer envelopes of AGB stars drives strong stellar winds, leading to additional dust condensation and mass loss, ultimately leading to complete loss of the envelope, leaving behind the inert core as a cooling white dwarf. The transition from AGB star to white dwarf corresponds to the beautiful planetary nebula stage; the nebula glow itself is caused by ionized gas in the expanding AGB outflow. As discussed below, a large fraction of the presolar oxide grains likely originated in O-rich AGB stars and were once fleetingly part of such spectacular displays.

Two additional processes that may affect the surface composition of AGB stars, and hence the compositions of presolar grains they produce, are "hot bottom burning (HBB)" and "cool bottom processing (CBP)." In HBB (Boothroyd et al., 1995), predicted to occur in AGB stars more massive than ~4–5$M_\odot$, the base of the envelope reaches temperatures high enough for H-burning reactions to occur, and convection then mixes the products throughout the envelope. CBP (Wasserburg et al., 1995; Nollett et al., 2003; Palmerini et al., 2011) has been hypothesized to occur in less massive (~1.75$M_\odot$) AGB stars and it mainly refers to a non-convective, conveyor-belt style mixing process, not predicted by standard stellar evolution calculations, in which material from the AGB envelope is mixed to hotter regions where it experiences some H-burning. The physical mechanism(s) responsible for CBP are as yet unknown, but magnetic-field induced buoyancy appears promising (Palmerini et al., 2021). In terms of isotopic signatures potentially observable in presolar oxide grains, both HBB and CBP will produce ^{17}O and ^{26}Al and destroy ^{18}O, as discussed in more detail later.

Stars more massive than about 10$M_\odot$ have very different evolutionary paths than LIMS (Chapter 8). Following core H- and He-burning, they become red supergiants. As in their lower-mass counterparts, convective mixing leads to enrichment of their envelopes in the products of partial H-burning (e.g., ^{14}N, ^{17}O). However, unlike LIMS, their cores are too massive to be supported by electron degeneracy pressure, so they experience a number of advanced burning stages (C-, Ne-, O-, and Si-burning) as succeeding fuels are consumed, resulting in an onion-like structure with increasingly processed material as one goes deeper into the star. Once Si-burning has resulted in a core dominated by Fe-group nuclei, no further energy generation by fusion reactions is possible. As a result, the star loses its battle against gravity and the core collapses until it is stabilized by neutron degeneracy, causing the

implosion to rebound and generate a massive shock wave, a "Type II supernova" explosion that accelerates most of the stellar material to escape velocity. As the shock wave passes through the star, additional nuclear reactions can occur throughout the ejecta. Thus, the isotopic and elemental composition at any point in the ejecta depends on its entire history of nuclear burning, both before and during the explosion, as well as any mixing that may occur between different zones (Meyer et al., 1995).

In terms of elements most relevant to presolar oxides, the most abundant isotope synthesized by Type II supernovae (hereafter SNII) is ^{16}O, and thus much of the SNII ejecta is dominated by material with very low $^{17}O/^{16}O$ and $^{18}O/^{16}O$ ratios (e.g., Rauscher et al., 2002). However, the outermost zones have O isotopic compositions reflecting H- and He-burning: the large H-rich envelope is ^{17}O-rich and somewhat ^{18}O-poor, the He- and N-rich zone that experienced complete H-burning is very ^{18}O-poor, and the He- and C-rich zone that experienced partial He-burning is ^{18}O-rich and ^{17}O-poor. These compositions, from a $20M_{\odot}$ SNII model (Woosley and Heger, 2007), are shown in Fig. 10a, with the percentage of the total ejected O from each zone indicated. The *gray region* indicates compositions that are possible from arbitrary mixing of the different SN zones. This mixing compositional space is huge and, in fact, overlaps a sizable proportion of the presolar oxide grains, except for the Group 1x grains. This points to the need for isotopic data for additional elements beyond O if one wants to accurately assess SNII as potential sources of specific presolar grains, as discussed in more detail later.

Mg similarly shows a wide range of isotopic compositions throughout the ejecta, as illustrated in Fig. 10b. The H envelope is predicted to be slightly ^{25}Mg-depleted and ^{26}Mg-enriched, due again to mixing of H-burning ashes. The C- and O-rich zone that experienced complete He-burning has very high $^{25}Mg/^{24}Mg$ and $^{26}Mg/^{24}Mg$ ratios, whereas these ratios decrease in inner zones, due to the production of ^{24}Mg by C-burning. Aluminum-26 is produced by H-burning in outer zones and by O- and Ne-burning in inner ^{16}O-rich zones, with the highest $^{26}Al/^{27}Al$ ratios of order 0.1 predicted for the He- and N-rich zone that experienced complete H-burning.

In recent years, M. Pignatari and coworkers have proposed modifications to standard models of SNII, in part to help better explain puzzling aspects of isotopic data for presolar SiC grains of probable supernova origin (Pignatari et al., 2013, 2015). In particular, they considered the effects of increasing the energy of the explosion compared to standard models and also considered the effects of mixing of a small amount of hydrogen into the convective He shell from above the shell. As the SN shock wave passes through the He shell, this H can be heated and undergo explosive H-burning, akin to that which occurs in classical nova explosions (see below). Although these models are parameterized and not yet tied to full hydrodynamical simulations, they have shown great promise for explaining both the cosmic origin of ^{15}N and a range of presolar SiC data (Pignatari et al., 2015; Liu et al., 2017). Moreover, such "H-ingestion supernovae" have been recently suggested as

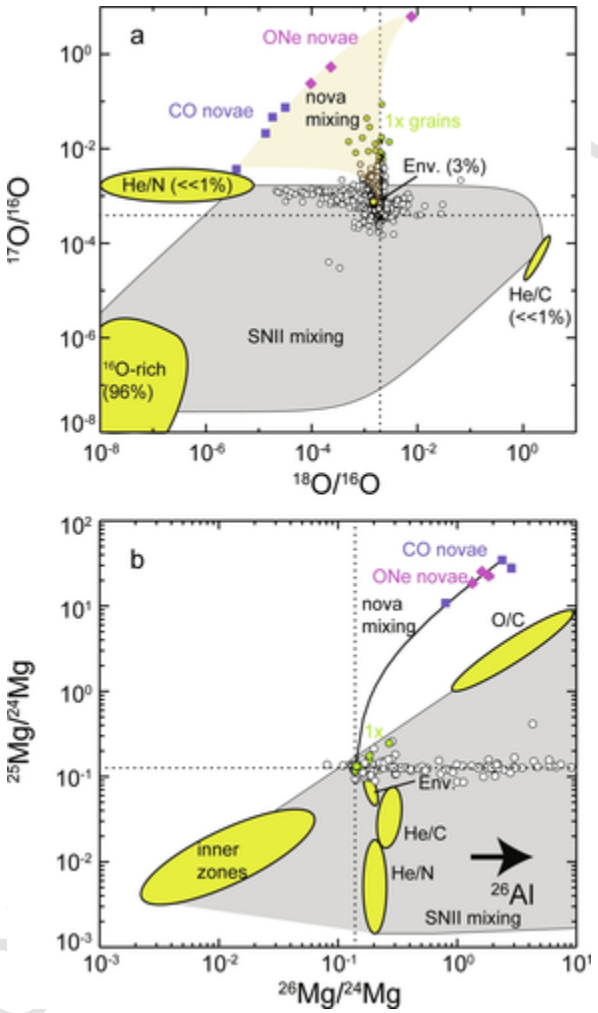

FIG. 10

The O- and Mg-isotopic compositions of presolar oxide grains are compared to predictions for nucleosynthesis in novae and supernovae. The *yellow ellipses* indicate ranges of compositions within different layers, specified by their most abundant elements and taken from a $20M_{\odot}$ SNII model (Woosley and Heger, 2007). Compositions of classical nova ejecta are predicted for explosions on white dwarfs of varying mass and composition (models calculated by J. Jose, reported by Gyngard et al., 2010a). The *dotted lines* indicate the terrestrial isotopic ratios.

sources of some presolar silicate grains (Leitner and Hoppe, 2019; Hoppe et al., 2021).

Classical novae are an additional potential site for production of presolar oxide grains. Novae are explosions which occur in close binary stellar systems, where one of the binary pair has evolved all the way through the AGB phase to become a white dwarf, which accretes material from its less evolved (main sequence or red giant) companion. The accreting H-rich material is heated to very high temperatures, eventually leading to a thermonuclear runaway that ejects nuclear processed material into the interstellar medium. The nuclear processing is dominated by proton reactions at very high temperatures ($2–3 \times 10^8$ K) and is thus often referred to as "explosive H-burning." Of importance here, calculated nova ejecta is characterized by large excesses of ^{17}O, a wide range of $^{18}O/^{16}O$ ratios depending on various characteristics of the nova (e.g., composition of white dwarf, degree of mixing between white dwarf and accreted material), extreme ^{25}Mg and ^{26}Mg excesses with $^{25}Mg/^{24}Mg \sim 10 \times {}^{26}Mg/^{24}Mg$, and very high $^{26}Al/^{27}Al$ ratios (>0.1). The predicted O isotopic ratios, based on one-dimensional hydrodynamical simulations of novae of different mass and white dwarf composition (Gyngard et al., 2010a), are shown in Fig. 10a. Although these all plot far from the presolar grain data, the tan area shows the possible composition space if the pure nova ejecta is mixed with material of terrestrial composition. As discussed later, the overlap of this mixing space with the highly ^{17}O-rich Group 1x oxide grains supports a possible nova origin for these grains.

The other major type of supernova explosions, called Type Ia, is extremely important for cosmology and as nucleosynthetic sources of iron-peak elements in the Universe. Typical SNIa are thought most likely to be nuclear explosions of white dwarfs, e.g., in binary systems like described above for novae, but with higher accretion rates such that the entire star explodes, rapidly converting the original C, O-rich material into Fe-peak elements. An alternative possibility is that SNIa form from mergers of two white dwarfs. SNIa are not observed to produce dust and thus have not often been considered as potential sources of presolar grains (Clayton et al., 1997). One exception is the suggestion that rare, "high-density" SNIa may be good sites for the nucleosynthesis of neutron-rich isotopes, like ^{48}Ca, ^{50}Ti, and ^{54}Cr (Meyer et al., 1996; Woosley, 1997), and thus potential progenitors of the ^{54}Cr-rich presolar nano-oxides identified in the Orgueil meteorite (Dauphas et al., 2010; Qin et al., 2011). More recent attention has been paid to "electron-capture supernovae" (ECSN)—a possible end-state of evolution of stars in the range of ~7–10$M_\odot$. Such stars have electron-degenerate cores of O, Ne, and Mg; if these grow massive enough, they may undergo electron capture reactions on ^{20}Ne, thereby losing degeneracy pressure and leading to a thermonuclear runaway. The resulting conditions are similar to those simulated for high-density SNIa and ECSN are thus an attractive potential source for neutron-rich isotopes (Wanajo et al., 2013) and ^{54}Cr-rich grains (Nittler et al., 2018; Jones et al., 2019).

5.2 Galactic chemical evolution

As galaxies evolve, new generations of stars are born, evolve, and expel newly synthesized nuclei into the interstellar medium (ISM). As a result, the chemical composition of stars varies with time and place, a process referred to as galactic chemical evolution (hereafter, GCE). A key parameter used in GCE studies is "metallicity," the mass fraction of elements heavier than He in a given mixture, usually expressed as Z. In the Sun, $Z = 0.014$ (Asplund et al., 2021). Of highest relevance to presolar grain studies is the distinction of "primary" isotopes, whose nucleosynthesis is metallicity-independent, and "secondary" ones, which can only be made in stars that already have some heavy elements. Thus, ^{16}O, which is made by He-burning, is a primary isotope, but ^{17}O, made by CNO-cycle H-burning, requires a star that already contains C, N, and O and thus is secondary. GCE theory predicts that the ratio of a secondary isotope to a primary one (e.g., $^{17}O/^{16}O$) increases roughly linearly with metallicity in a galaxy (e.g., Clayton, 1988), a notion supported by measurements of O isotopes in molecular clouds (Penzias, 1981). GCE is thought to play a key role in explaining the Si and Ti isotopic systematics of many presolar SiC grains (Timmes and Clayton, 1996; Alexander and Nittler, 1999; Nittler and Dauphas, 2006) and the O, Mg, and Ca isotopes in presolar oxides and silicates (especially Group 1 and 3 grains) as discussed below.

5.3 Origins of group 1 and 2 presolar oxide grains

The O isotopic ratios of most presolar oxide grains are shown again in Fig. 11, along with the ratios measured spectroscopically in the envelopes of evolved stars (Harris and Lambert, 1984a; Harris et al., 1985; Smith and Lambert, 1990; Lebzelter et al., 2015), including O- and C-rich AGB stars, Ba stars (thought to be red giant stars that have experienced mass transfer from a now-dead AGB companion), and two red supergiants (Antares and Betelgeuse). It is immediately apparent that there is a strong overlap between the stellar data and the Group 1 grains. This observation, along with evidence from astronomical observations that AGB stars are the largest contributors of dust to the interstellar medium (Gehrz, 1989) and that O isotopes and inferred initial $^{26}Al/^{27}Al$ ratios were in the range of model calculations, led to the conclusion that Group 1 grains most likely originated in outflows from RGB and AGB stars (Boothroyd et al., 1994; Nittler et al., 1994). Following further studies on the nature and sources of interstellar dust (Kemper et al., 2004), Nittler et al. (2008) noted that up to 15% of Group 1 grains may have originated from massive stars during a red supergiant phase. More recently, Mg-isotopic anomalies in some Group 1 presolar silicate grains have led to the suggestion that a substantial fraction may in fact have formed in Type II supernova explosions (Leitner and Hoppe, 2019). We thus consider in more detail here the Group 1 (and 2) presolar grain oxide data in light of the current understanding of these potential stellar sources.

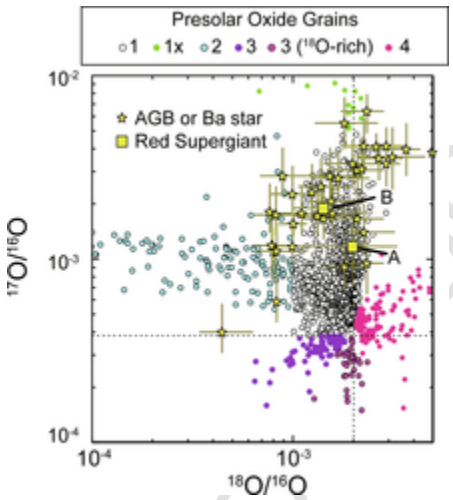

FIG. 11

Oxygen isotopes of many presolar oxide grains compared to those measured spectroscopically in AGB stars, Ba stars, and *red supergiants* (A = Antares, B = Betelgeuse). The dotted lines indicate the terrestrial isotopic ratios.

- Stellar data are from Harris, M.J., Lambert, D.L., 1984a. Oxygen isotopes in the atmospheres of Betelgeuse and Antares. Astrophys. J. 281, 739–745; Harris, M.J., Lambert, D.L., Smith, V.V., 1985. Oxygen isotopic abundances in evolved stars. I. Six barium stars. Astrophys. J. 292, 620–627; Smith, V.V., Lambert, D.L., 1990. The chemical composition of red giants. III. Further CNO isotopic and s-process abundances in thermally pulsing asymptotic giant branch stars. Astrophys. J. Suppl. 72, 387–416; Lebzelter, T., Straniero, O., Hinkle, K.H., Nowotny, W., Aringer, B., 2015. Oxygen isotopic ratios in intermediate-mass red giants. Astron. Astrophys. 578, A33.

In Fig. 12, we compare O and Al-Mg isotopic data for presolar oxide grains with various model predictions. First dredge-up curves (FDUP, see Fig. 9) for two metallicities and a range of stellar masses, taken from Boothroyd and Sackmann (1999), are shown in Fig. 12a. The initial compositions of the model stars were assumed to vary with metallicity according to GCE theory (*black arrow*). It is clear that the FDUP can explain the ^{17}O enrichments and ^{18}O depletions seen in Group 1 grains (and AGB stars in Fig. 11), provided that the grains formed in stars with a range of masses (to explain the spread in $^{17}O/^{16}O$) and initial compositions (to explain that in $^{18}O/^{16}O$). The simplest explanation for the spread in initial compositions is that the parent stars sampled a range of metallicities, and as discussed in the previous section, the $^{17}O/^{16}O$ and $^{18}O/^{16}O$ ratios of new stars are expected to increase proportionally with metallicity due to GCE (*black arrow* in Fig. 12a). The shape of the FDUP curve (Fig. 9a) would, in principle, allow for grains with $^{17}O/^{16}O > 2 \times 10^{-3}$ to have originated in stars of mass 2–7$M_\odot$. However, as discussed in Section 5.1 and further below, AGB stars more massive than about 4$M_\odot$ are expected to undergo hot bottom burning (HBB) and thus have much more ex-

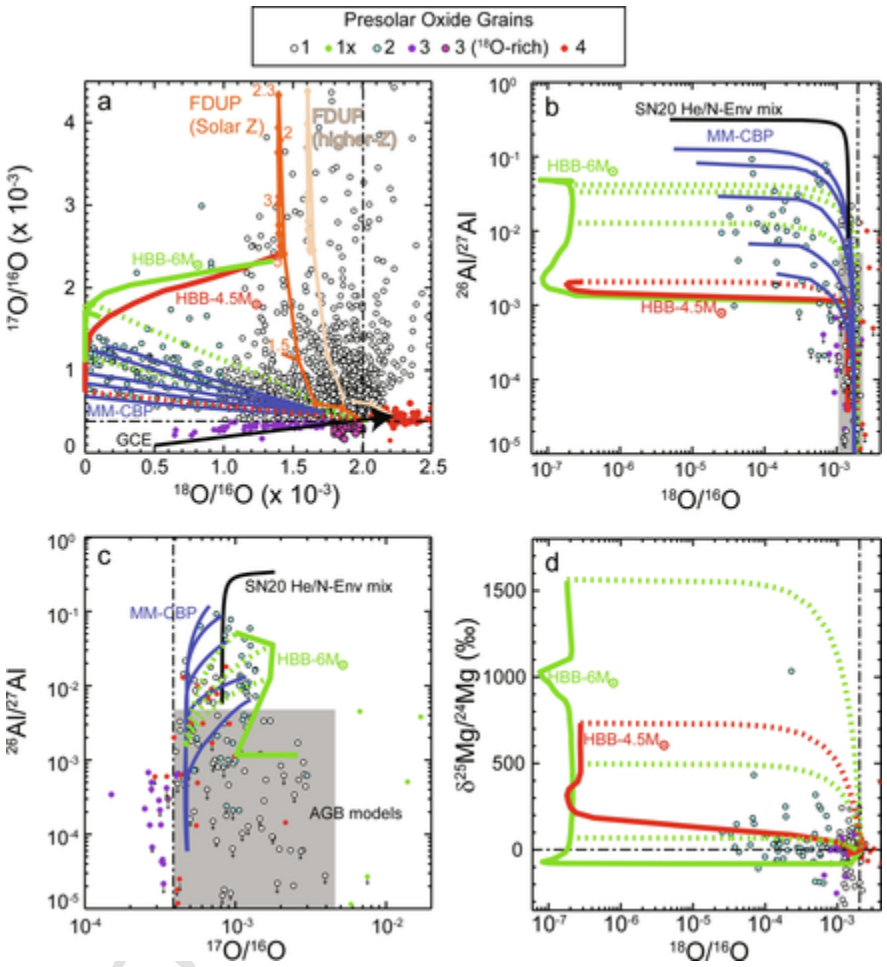

treme ^{18}O depletions. Therefore, Group 1 grains with $^{17}O/^{16}O$ in this range more likely formed in lower mass stars. Nittler (2009) showed that the O-isotopic distribution of Group 1 (and 3) grains was reasonably well explained by expectations of GCE theory if the grain parent stars had a maximum mass of ~2.2$M_{\odot}$. Above this mass (and below the HBB limit), AGB stars are more likely to become C-rich due to dredge-up of ^{12}C from the He shell and thus condense carbonaceous grains rather than oxides.

If one accepts that a given grain most likely formed in an RGB or AGB star that has experienced the FDUP, one can compare its O isotope ratios to a grid of predicted ratios for varying masses and metallicities (e.g., that of Boothroyd and Sackmann, 1999) to infer the mass and metallicity of its parent star, as has been done in several studies (Alexander and Nittler, 1999; Nittler, 2009). The validity of such an

exercise depends on the validity of the assumption that the $^{18}O/^{16}O$ ratio of the parent star is determined mainly by its initial composition only slightly modified by the FDUP. However, the strong ^{18}O depletions observed in Group 2 grains strongly suggest that additional processing may well affect a star's $^{18}O/^{16}O$ ratio. As discussed in Section 5.1, two additional mixing processes in AGB stars may cause a decrease in $^{18}O/^{16}O$: cool-bottom processing (CBP) in low-mass AGB stars and HBB in intermediate-mass stars.

Shown as *blue curves* in Fig. 12 are predicted isotopic ratios for a model of magnetic mixing-induced CBP in a $1.2M_{\odot}$ AGB star (Palmerini et al., 2017, 2021); each curve corresponds to a different value of a model parameter related to plasma density (and, indirectly, depth of mixing). It is clear from Fig. 12a that such models can easily explain most of the spread of O isotopes in Group 2 grains as well as many Group 1 grains with relatively low $^{17}O/^{16}O$ ratios. The *solid red and green curves* show predictions for HBB in 4.5 and $6M_{\odot}$ stars, respectively, from Lugaro et al. (2017). Although these curves intersect a very small number of relatively ^{17}O-rich Group 2 grains, HBB rapidly leads to extremely low $^{18}O/^{16}O$ ratios (essentially zero), below most of the grain data. However, Lugaro et al. (2017) pointed out that if these compositions were mixed with solar-like material, the mixtures would overlap well with the Group 2 grain O-isotope data (*red and green dotted lines*). Note that predictions of stellar nucleosynthesis depend critically on the reaction rates for the various nuclear reactions involved and many of these are still relatively poorly constrained by laboratory measurements at the relevant stellar energies. In particular, the $^{17}O/^{16}O$ ratio produced by the H-burning CNO cycle depends on the still uncertain cross sections for $^{17}O+p$ reactions, and the HBB and CBP predictions shown in Fig. 12 were calculated with different sets of reaction rates. In any case, it appears that the stellar origins of Group 1 and 2 grains cannot be resolved on the basis of O isotopes alone, so let's turn to other isotope systems for additional constraints on the grain origins.

In Fig. 12b and c, we compare the inferred $^{26}Al/^{27}Al$ ratios for the grains as a function of O isotopes to the model predictions. The *gray shaded regions* show the

FIG. 12

The isotopic compositions of presolar oxide grains are compared to predictions for nucleosynthesis in AGB stars and supernovae. FDUP = predicted first dredge-up composition for stars of $1–7M_{\odot}$ and two metallicities (Boothroyd and Sackmann, 1999). Numbers on the Solar-Z FDUP curve indicate stellar mass in solar masses. HBB = predicted compositions for AGB stars of $4.5M_{\odot}$ (*red*) and $6M_{\odot}$ (*green*); the *solid curves* are the envelope composition; *colored dotted lines* indicate mixing with solar-like material (Lugaro et al., 2017). MM-CBP curves are the predicted envelope composition for a $1.2M_{\odot}$ AGB star undergoing cool-bottom processing via a magnetic-mixing model (Palmerini et al., 2021). The HBB and CBP predictions were calculated with different sets of reaction rates. The *black curves* indicate mixing between the H-rich envelope and He/N zone of a $20M_{\odot}$ Type II supernova (Woosley and Heger, 2007). The *gray shaded regions* in (B) and (C) show the predicted range of isotope ratios for standard low-mass AGB star models, i.e., without CBP. The *dash-dot lines* indicate terrestrial isotopic ratios.

predicted range of isotope ratios for standard low-mass AGB star models, i.e., without CBP. The most recent calculations for low-mass AGB star ^{26}Al production predict maximum envelope ^{26}Al/^{27}Al ratios of a few times 10^{-3} (Karakas and Lugaro, 2016). Many Group 1 grains, especially those with ^{17}O/^{16}O > 10^{-3}, are in good agreement with the standard low-mass AGB models for ^{26}Al/^{27}Al. Moreover, unlike the case for presolar silicates (Leitner and Hoppe, 2019; Hoppe et al., 2021), very few Group 1 or 2 oxides show large ^{25}Mg excesses that may point to a massive AGB or Type II supernova origin. These observations support the long-standing idea that low- and/or intermediate-mass O-rich AGB stars are the parents of these grains. A few Group 1 presolar spinel grains do, however, show unusual ^{25}Mg depletions and ^{26}Mg excesses (Fig. 6c; Gyngard et al., 2010b), a signature also seen in some Group 1, 2, and 4 oxides and silicates. Hoppe et al. (2021) have proposed either a red supergiant wind or Type II supernova ejecta origin for such ^{25}Mg-poor Group 1 grains. These grains make up a few percent of the Group 1 oxides measured for Mg isotopes, and thus these sources may have contributed a similar proportion to the Group 1 presolar oxide population.

Fig. 12b and Cc clearly shows that many Group 2 grains and Group 1 grains with ^{17}O/^{16}O < 10^{-3} have inferred ^{26}Al/^{27}Al ratios higher than the predictions for standard low-mass AGB star nucleosynthesis (*gray area*). This provides further strong evidence that Group 1 grains with ^{17}O/^{16}O and ^{26}Al/^{27}Al in this range are more likely related to Group 2 grains and arise from the same stellar sources. The data are consistent with predictions for magnetic-mixing CBP (*blue curves*). As is the case for O isotopes, the HBB predictions (*solid green* and *red curves*) largely miss the Group 2 data but overlap with the grains if the pure HBB composition is mixed with solar composition (*green and red dotted curves*). That CBP does not require such additional mixing may be an argument in favor of low-mass AGB stars experiencing CBP as the sources of Group 2 grains, but the relatively large ^{25}Mg excesses in a few Group 2 oxides (e.g., Lugaro et al., 2007; Nittler et al., 2008) are more consistent with more massive HBB-AGB stars (e.g., Fig. 12d). As implied by Fig. 10, an additional possibility for Group 2 grains would be mixing of envelope material with the partially H-burnt He/N shell in Type II supernovae. However, such mixing completely misses the Al-Mg grain data (e.g., Fig. 12b) and supernovae are thus unlikely as sources of the Group 2 (and ^{26}Al-rich Group 1) grains.

From the above discussions, we can conclude that AGB stars are most likely the dominant sources of Group 1 and 2 grains. The range of inferred ^{41}Ca/^{40}Ca ratios for presolar hibonite grains is also in reasonably good agreement with low-mass AGB models (Nittler et al., 2008). However, this is not the case for ^{25}Mg/^{24}Mg or stable Ca or Ti isotope ratios, where the observed anomalies do not in general match predictions of AGB nucleosynthesis. As mentioned above, some of the more extreme ^{25}Mg excesses and depletions may point to origins of a small fraction of Group 1 grains in more massive AGB stars or supernovae. On the other hand, just as GCE is thought to play an important role in setting the initial ^{18}O/^{16}O ratios of Group 1 parent stars, so it should also affect Mg, Ca, and Ti isotopes since ^{24}Mg, ^{40}Ca, and ^{48}Ti are primary isotopes and the rarer isotopes of these elements are

mostly secondary (Section 5.2). In Fig. 13, we plot some Mg, Ca, and Ti isotope ratios against the solar-normalized inferred initial $^{18}O/^{16}O$ ratios (or equivalently, metallicity Z) of Group 1 grains. The latter were estimated from the grains' O isotopes and the first dredge-up models of Boothroyd and Sackmann (1999). However, compared to previous work (Nittler et al., 2008), they were additionally increased by ~10% to take into account recent models (e.g., Fig. 9b; Karakas and Lugaro, 2016) that predict slightly more depletion of ^{18}O during the FDUP than calculated

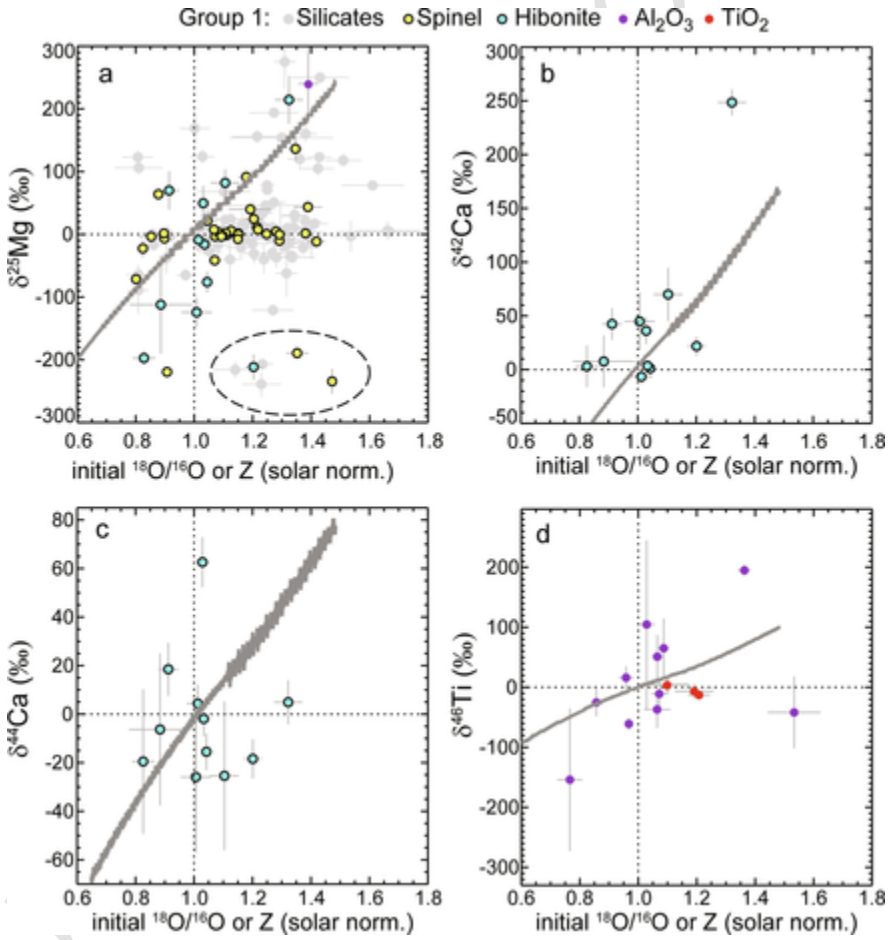

FIG. 13

The isotopic compositions of presolar oxide and silicate grains are compared to predictions of galactic chemical evolution (GCE, *gray curves* taken from Kobayashi et al., 2011). *X*-axis is the solar-normalized initial $^{18}O/^{16}O$ ratio for each grain, extrapolated from the models of Boothroyd and Sackmann (1999), assumed to vary linearly with metallicity *Z*.

by Boothroyd and Sackmann (1999). These values are clearly model-dependent but still useful for qualitatively investigating the hypothesis that GCE is a strong driver of isotope ratios in presolar oxide grains. The *gray curves* are predicted GCE trends from the model of Kobayashi et al. (2011), renormalized to match solar composition at solar metallicity, a procedure discussed originally for Si-isotope GCE by Timmes and Clayton (1996). Note that such GCE calculations are subject to many uncertainties associated with both the assumptions underlying the Galactic evolution model (e.g., the initial mass function for new stars) and input physics, from stellar lifetimes to nucleosynthetic yields for each relevant isotope for different types of stars. For example, Vangioni and Olive (2019) recently presented models for the GCE of Mg isotopes showing a very wide range of predictions depending on various stellar yields and assumed initial mass functions.

If the Mg, Ca, and Ti isotopes of the grain parent stars were determined by homogeneous GCE, one would expect tight correlations among the grain data in Fig. 13 which could then be used to test GCE models (e.g., the gray trends). However, this is clearly not the case for most of the plotted data. First, considering $^{25}Mg/^{24}Mg$ (Fig. 13a), most hibonites and one ^{25}Mg-rich presolar Al_2O_3 grain plot relatively close to the predicted GCE trend. However, although some spinel and silicate grains do as well, these types also show much more scatter, with three populations of grains that plot far from the GCE trend: (1) a large fraction of grains having $\delta^{25}Mg$ within errors of zero, independent of the initial $^{18}O/^{16}O$ ratio, (2) a population of grains with much higher ^{25}Mg excesses than predicted, and (3) a population of grains (dashed ellipse) depleted in ^{25}Mg, but with high inferred metallicity. Given that the Solar Mg isotopic composition does not obviously hold any particular cosmic significance, the presence of grains with highly anomalous O isotopes but normal Mg (population 1) is somewhat surprising. Nittler et al. (2008) proposed that presolar spinel grains with normal Mg may have experienced isotopic exchange in space or on the meteorite parent bodies and this has been suggested for some presolar silicates as well (Hoppe et al., 2018). If this is indeed the explanation for the normal grains, the lack of hibonite grains with such signature likely indicates that hibonite is more resistant to Mg isotope exchange than spinel or silicates; this is presumably testable via laboratory experiments. As mentioned above, grains in population (2) have been argued to originate not from low-mass AGB stars, but rather Type II supernovae and/or massive AGB stars (Leitner and Hoppe, 2019; Hoppe et al., 2021). However, Nittler et al. (2008) suggested an alternative route to ^{25}Mg-rich grains with Group 1 or 2 isotope signatures, namely mass transfer from an evolved intermediate-mass binary AGB companion to a lower mass star that eventually evolves to the AGB phase and condenses the grains. All of these scenarios merit further investigation. Population (3) grains correspond to the same ^{25}Mg-depleted, ^{26}Mg-enriched grains discussed earlier and postulated to form in red supergiants or supernovae (Hoppe et al., 2021).

Even if we assume that the grains that do show rough correlation in Fig. 13a indeed preserve a record of GCE, there is still substantial scatter around any trend, making comparison with GCE predictions difficult. Heterogeneity in GCE is ex-

pected due to the stochastic nature of star formation and non-negligible mixing timescales in the interstellar medium (e.g., Lugaro et al., 1999; Nittler, 2005) and this scatter may well reflect such inhomogeneities around an average trend. Spectroscopic measurements of Mg isotopes in main-sequence stars also show more scatter than GCE theory would predict (e.g., Gay and Lambert, 2000; Yong et al., 2003; Meléndez and Cohen, 2007), although uncertainties are much larger than can be achieved by laboratory measurements of presolar grains.

The more limited datasets for Ca and Ti isotopes in presolar oxide grains (Fig. 13b–d) limit the ability to compare with GCE theory. Nonetheless, there are hints of trends for $^{42}Ca/^{40}Ca$, $^{43}Ca/^{40}Ca$ (see Nittler et al., 2008), and $^{46}Ti/^{48}Ti$, albeit with significant scatter, again possibly attributable to heterogeneous GCE. Of all the measured Ca and Ti isotopes in Group 1 presolar oxide grains, $^{44}Ca/^{40}Ca$ shows the least correlation with inferred metallicity (Fig. 13c). As discussed by Nittler et al. (2008), this is likely a consequence of the fact that a significant portion of ^{44}Ca is synthesized in rare supernova events which may be expected to contribute inhomogeneously to the interstellar medium. In any case, it is clear that far more multielement isotope data for Group 1 presolar grains are needed if the grains are to be a truly useful tool for testing GCE models. Recent progress on this front has come from correlated Mg- and Si- isotopic measurements of presolar silicates (Hoppe et al., 2018, 2021).

To summarize this section, based on multielement isotopic data for Group 1 and 2 presolar oxide grains, we can conclude that most of these grains formed in AGB stars, low-mass ($<2M_{\odot}$) ones for Group 1 grains with $^{17}O/^{16}O > 10^{-3}$, and either low-mass ones experiencing cool-bottom processing or intermediate mass ones experiencing hot bottom burning for the Group 2 grains and some Group 1 grains with lower ^{17}O enrichments. Resolving the mass range of the Group 2 parent stars will depend on further progress in laboratory measurements of key nuclear reaction rates and in AGB star modeling. A small fraction of Group 1 grains likely formed in red supergiant winds or supernova ejecta and a small number of ^{25}Mg-rich Group 1 and 2 grains may have formed in supernovae, massive AGB stars, or stars that experienced mass transfer from a massive AGB companion. GCE is likely imprinted in several isotopic systems measured in the grains, but far more work is needed to use the grain data to test GCE models.

5.4 Origins of ^{18}O-poor group 3 presolar oxide grains and the age of the galaxy

As discussed in Section 4.1, Group 3 grains lie in the ^{16}O-rich quadrant of the O 3-isotope plot and can be further subdivided based on their $^{18}O/^{17}O$ ratios. Grains with $^{18}O/^{17}O$ greater than the Solar ratio are referred to here as "^{18}O-rich Group 3 grains" and will be discussed in the following section. As seen in Fig. 12a, the "regular" Group 3 grains lie above the model GCE trend for O isotopes. It was thus recognized early on (Nittler et al., 1994) that, like Group 1 grains, their compositions could also be explained by the first dredge-up in AGB stars, provided that they

formed in stars (1) that had initial $^{17}O/^{16}O$ and $^{18}O/^{16}O$ ratios lower than Solar and (2) were of low enough mass that the FDUP did not increase their envelope ^{17}O contents too much (e.g., Fig. 9a). Lower initial $^{17,18}O/^{16}O$ ratios would be expected for stars of lower-than-Solar metallicity, reflecting GCE, and therefore low-metallicity, low-mass AGB stars have long been accepted as the most likely sources of Group 3 grains. In fact, since the main sequence lifetimes of stars decrease steeply with increasing mass and presolar grains formed at the end of the parent stars' lives, lower-mass presolar grain progenitors would on average be expected to have formed earlier in Galactic history than higher-mass ones and thus more likely be of lower metallicity. Nittler et al. (1997) and Nittler (2009) showed that the overall shape of the Groups 1 and 3 O-isotope distribution can be naturally explained by simple GCE considerations and FDUP predictions, lending further support to the idea that the grains originated in low-mass, low-metallicity AGB stars. Based on comparison with the FDUP predictions, Group 3 grains can be inferred to have originated in stars roughly of mass 1.15–1.35$M_{\odot}$ and metallicities down to one-half Solar.

Based on the long lifetimes of such low-mass stars, Nittler and Cowsik (1997) argued that the Group 3 presolar oxide grains can be used as an independent method of estimating the age of the Milky Way Galaxy. The basic concept is simple: presolar grains formed before the formation of the Sun 4.6 Gyr ago and their parent stars formed some period of time before that, so the age of the Galaxy has to be longer than the longest age inferred for a grain parent star plus the age of the Solar System. Moreover, the Galaxy formed with much lower metallicity than inferred for the parent stars, so the grains also require that the Galaxy had evolved for some time before even the oldest parent formed. This is of course a highly model-dependent exercise, but the age obtained of 14.4 ± 1.3 Gyr (and probable systematic errors of several billion years) is in remarkable agreement with completely independent estimates based on cosmological and/or astronomical measurements.

The primary difficulty with a low-mass, low-metallicity AGB star origin for the Group 3 grains is that it is based essentially entirely on O isotopes, as very little data have been reported for other elements for these grains, making it difficult to test different possible stellar origins. Mg isotopes have been reported for a couple of dozen Group 3 Al_2O_3, spinel, and hibonite grains, but almost all have shown normal isotopic compositions, including little evidence for extinct ^{26}Al (Nittler et al., 1997; Choi et al., 1999; Zinner et al., 2005; Gyngard et al., 2010b). In an abstract, Nittler et al. (2011) reported large Mg and Ca isotopic anomalies in a Group 3 hibonite grain. The observed pattern—depleted in ^{25}Mg, enriched in ^{41}K, ^{42}Ca, ^{43}Ca, and ^{44}Ca—is more suggestive of a supernova source (Section 5.5) than a low-mass AGB star, but these authors were unable to obtain a satisfactory mixture of supernova material to match the grain's composition. Clearly, much more multielement isotopic data for Group 3 grains are needed to resolve their stellar origins.

5.5 Origins of group 4, ^{18}O-rich group 3, and ^{16}O-rich presolar oxide grains

Soon after ^{18}O-rich Group 4 presolar oxides were first discovered, three possible sources were proposed (Nittler et al., 1997; Choi et al., 1998): (1) low-mass AGB stars for which early third dredge-up episodes could mix ^{18}O produced by partial He-burning into the envelope, (2) high-metallicity AGB stars, in which case high ^{18}O/^{16}O ratios reflect GCE (GCE), and (3) Type II supernovae. The first suggestion was soon discounted since no AGB models predict third dredge-up to occur during the very early thermal pulses when ^{18}O may be abundant below the H-burning shell. A supernova origin is generally held to be most likely for most Group 4 grains, but high-metallicity AGB stars remain a possibility, at least for some grains. Here we consider the arguments and evidence for these two possible stellar sources.

As discussed in Section 5.1 and shown in Fig. 12a, the He- and C-rich zone of a SNII is highly enriched in ^{18}O and depleted in ^{17}O, due to partial He-burning. In contrast, most Group 4 oxide grains have Solar or higher ^{17}O/^{16}O ratios. Choi et al. (1998) first suggested that this isotope signature could reflect mixing in supernova ejecta of material from the He/C zone with material from the envelope and He/N zones, both of which are ^{17}O-enriched due to H-burning. These authors showed that mixing of predicted compositions for specific zones of a $15M_{\odot}$ SNII model could well reproduce most of the O, Mg, Ca, and Ti isotopic ratios measured in a Group 4 Al_2O_3 grain, though most of the Ca and Ti ratios were Solar within large errors. The discovery of a ^{17}O-poor, ^{18}O-rich presolar silicate grain (Fig. 2a; Messenger et al., 2005) gave further credence to a SNII origin for the ^{18}O-rich grains. The strongest evidence for a SNII origin for at least some Group 4 grains came with the discovery of a Group 4 hibonite grain, KH2, for which many isotopic ratios could be measured (Nittler et al., 2008). These authors found that mixing material from six zones of a $15M_{\odot}$ supernova could reproduce 7 out of 8 measured isotopic ratios to a high degree of accuracy (Fig. 14); the model includes the effect of ^{26}Al on the ^{26}Mg/^{24}Mg ratio. As might be expected from comparison of the grain's O isotopic composition to the SN zone compositions (Fig. 10a), the mixture is dominated by material from the massive star's H-rich envelope and the immediately underlying He-rich zones. Unlike the original mixing calculation of Choi et al. (1998), however, material from inner zones is required to explain all the observed isotope signatures, though the amount is necessarily very small since these zones are dominated by ^{16}O produced by core He-burning, making up >95% of the ejected oxygen, so only a tiny amount can have a large effect on mixed isotopic compositions. Nittler et al. (2008) demonstrated that similar mixing calculations could also explain the compositions of two Group 4 spinel grains, though with only O and Mg isotopic ratios, the problem is not nearly as well constrained. Nevertheless, these authors argued that the successful matching of the mixing models to the compositions of three grains makes a SNII source most likely for most or all Group 4 grains, and this view has generally taken hold in the community. For example, simi-

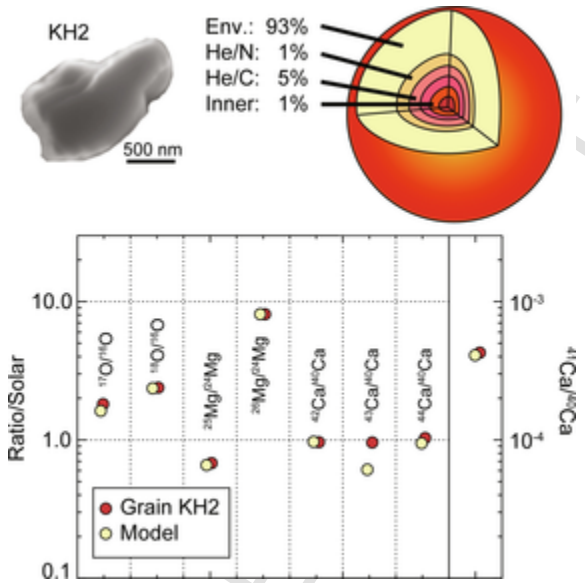

FIG. 14

Supernova mixing can explain the composition of presolar hibonite grain KH2 (Nittler et al., 2008). Top left: scanning electron microscope image of KH2. Top right: cartoon indicating relative amounts of different zones of a Type II supernova that can match the grain's composition. Bottom: a comparison of predicted isotopic compositions to observed compositions indicates excellent agreement for seven out of eight isotopic ratios, supporting a supernova origin for KH2 and the other Group 4 grains.

lar mixing calculations have been performed to explain O, Mg, Si, and/or Fe isotope systematics in Group 4 presolar silicate grains (Nguyen and Messenger, 2014; Hoppe et al., 2021).

As mentioned above, the proposal that Group 4 grains could instead have originated in high-metallicity AGB stars reflects the expectation that such stars are born with $^{17}O/^{16}O$ and $^{18}O/^{16}O$ ratios higher than Solar, due to GCE. Nittler et al. (1997, 2008) argued that such an origin is unlikely for two reasons. First, while a majority of the Group 4 presolar oxide grains are ^{17}O-enriched, their O isotopic compositions generally lie near an extension of the predicted GCE trend, but FDUP in the parent stars would be expected to lead to higher $^{17}O/^{16}O$ ratios, as seen in Group 1 (and Group 3, if these are indeed from low-metallicity AGB stars, see previous section) grains. This problem is even more severe for the population of grains with $^{17}O/^{16}O$ near to or lower than Solar, as this would require that the parent stars formed far below the GCE trend. Second, the highest $^{18}O/^{16}O$ ratios observed (up to 10 s times the Solar ratio) would require extremely high metallicities, and such stars are unlikely to have been abundant at the time of the Sun's birth (and would have

required to have formed much earlier in Galactic history, when the average metallicity was lower). However, only some 15%–30% of Group 4 oxides would require an origin in stars of >2 times solar metallicity, depending on whether grains with compositions in the range of cosmic symplectite (Fig. 2b) are considered to be presolar grains. Moreover, Lugaro et al. (2020) have argued recently for an origin for most µm-sized presolar SiC grains in high-metallicity AGB stars, 2–3$Z_{\odot}$, on the basis of Sr isotope measurements of SiC, observations of stars, and models. Therefore, it may not be unreasonable to expect some oxide grains from high-metallicity AGB stars as well. The first problem regarding ^{17}O remains, however.

As an example of the ambiguity in deducing the stellar origins of some Group 4 presolar grains, consider the Group 4 presolar magnesiowüstite ((Mg,Fe)O) grain, 34C-10, reported by Floss et al. (2008). This grain has a moderate (34%) excess in ^{18}O/^{16}O, normal ^{17}O/^{16}O, and 10%–20% depletions in ^{54}Fe and ^{57}Fe, relative to ^{56}Fe. For comparison, the hibonite grain KH2, for which a supernova was suggested above, has much larger excesses of both ^{17}O and ^{18}O. Floss et al. (2008) discussed both AGB stars and supernovae as possible sources, but showed that neither fits the isotopic data particularly well. The combined depletions of ^{57}Fe and ^{54}Fe are not expected for super-Solar metallicity AGB stars; for example, Kobayashi et al. (2011) predict that ^{54}Fe/^{56}Fe increases with metallicity. Supernova mixtures that match the O isotopic composition of this grain predict ~solar Fe isotopic ratios. One part of a SN zone was found to be depleted in both ^{54}Fe and ^{57}Fe, but since this zone is also highly ^{16}O-rich, it was not possible to simultaneously match the grain's Fe and O isotopes. In the end, Floss et al. (2008) came down slightly in favor of an AGB origin for grain 34C-10, not because of isotopic considerations but because of astronomical evidence for this oxide phase to be present around such stars.

As discussed in Section 4.1, ^{18}O-rich Group 3 grains are those that have ^{18}O/^{17}O ratios higher than the Solar ratio. Because this ratio is only decreased by the first dredge-up, it is very unlikely that these grains formed in AGB stars and Nittler et al. (2008, 2020) suggested they may be related to Group 4 grains and have formed in Type II supernovae. This is certainly feasible from an O isotopic point of view (Fig. 10a) as mixing of SN zones can match their compositions, but as we have seen with some other populations, the lack of isotopic data apart from O in these grains makes it impossible to convincingly test this hypothesis. Mg isotope data were reported for two ^{18}O-rich Group 3 presolar spinel grains, but found to be normal, likely indicating isotopic exchange, as discussed earlier, and thus not highly diagnostic.

Nittler et al. (1998) reported a highly ^{16}O-rich presolar Al_2O_3 grain from the Tieschitz ordinary chondrite meteorite. Because ^{16}O is the main product of nucleosynthesis in Type II SNe, these authors argued that a supernova was the most likely source for this grain. This was confirmed by the discovery of another ^{16}O-rich oxide, a spinel grain which also showed a large ^{25}Mg depletion and a ^{44}Ca excess (Gyngard et al., 2010b), almost certainly pointing to in situ decay of ^{44}Ti. Because the latter isotope has a half-life of some 60 years and is only produced in SNe, its inferred presence in a presolar grain has long been taken as strong proof of

a supernova origin (Nittler et al., 1996). Given that SNII are such prodigious producers of ^{16}O (e.g., Fig. 10a), it is perhaps not surprising to find presolar grains with this composition. In fact, the rarity of such grains within the presolar oxide database remains a major mystery. As discussed above, there is clear evidence that many Group 4 grains (and maybe some Group 1 grains) originated in supernovae, but the compositions of these grains indicate a formation primarily from the outer layers, which are primarily composed of H and He, and not the inner zones which contain by far the greatest mass of the condensable elements in the supernova ejecta. For example, if all of the Mg, Al, and Si in the envelope of a $25M_{\odot}$ SN (Woosley and Heger, 2007) condensed into oxide and silicate grains, the total mass would be $\sim 0.05M_{\odot}$, whereas the same elements from the O-rich inner ejecta would sum to $\sim 0.9M_{\odot}$ of dust if there was 100% condensation. Estimates of dust production in SNII from astronomical observations are typically up to a few tenths of a solar mass (Indebetouw et al., 2014; De Looze et al., 2017), much higher than possible from condensation in the outer zones alone.

There are at least two possible explanations for the fact that the presolar grain population does not reflect the expectation that SN dust should be dominated by ^{16}O-rich grains from inner zones: (1) If ^{16}O-rich SN grains are produced with steeply decreasing size distributions and typical sizes much smaller than ~100 nm, they would be underrepresented in the known presolar grain data, as searches to date for presolar oxides have been almost entirely conducted at larger spatial scales (e.g., Fig. 4). (2) Newly formed ^{16}O-rich grains deep inside SN ejecta may be destroyed by encounters with reverse shock waves due to the original SN shock reflecting off the nearby circumstellar medium (e.g., Nozawa et al., 2007). In fact, these two possibilities may go hand in hand. Recent modeling of dust in the Cassiopeia-A SN remnant (Priestley et al., 2022) indicates that grains >200 nm will largely survive reverse shocks, while smaller ones are preferentially destroyed. Thus, if larger grains are formed in outer layers of the SN ejecta than in the inner layers, the ^{16}O-rich grains are likely to be preferentially destroyed. We note that the question of how much dust SNe produce is of great interest and debate in the cosmology community since large dust masses are observed in galaxies at high redshifts (Bertoldi et al., 2003; Watson et al., 2015), which have not had sufficient time to evolve to the point of having numerous AGB stars injecting dust into their interstellar media. Better understanding of the relative populations of presolar SN grains of different types and sizes may well help resolve this question in the future.

5.6 Origins of group 1x presolar oxide grains

Group 1x grains are highly enriched in ^{17}O with $^{17}O/^{16}O$ ratios higher than predicted for AGB star envelopes, 0.005–0.1 and $^{18}O/^{16}O$ ratios in the range of other Group 1 grains (Figs. 5 and 9). The first discovered 1x grain, alumina grain T54, was proposed to have formed in an intermediate-mass AGB star undergoing HBB (Nittler et al., 1997), with its relatively high measured $^{18}O/^{16}O$ ratio perhaps being caused by contamination on the sample mount. The subsequent discovery of several

more such grains for which substantial contamination could be ruled out argues against this HBB scenario. At the time of that work, nova nucleosynthesis calculations reproduce the high ^{17}O enrichment of T54, but predicted much higher $^{18}O/^{16}O$ ratios than observed in the grain (e.g., Politano et al., 1995). However, subsequent nova models predicted a much wider range of $^{18}O/^{16}O$, from subsolar to super-solar (José et al., 2004; Gyngard et al., 2010a), leading to the suggestion that Group 1x grains could in fact originate in such sources (Gyngard et al., 2010a). As seen in Fig. 10a, mixing of ejecta from CO and ONe novae of different masses with isotopically Solar material can reproduce the range of observed O isotopes in the Group 1x grains. A few Group 1x grains have ^{25}Mg and ^{26}Mg excesses as predicted for nova nucleosynthesis. However, their Mg isotope ratios do not match expectations for mixing of nova ejecta with solar material. A couple of Group 1x presolar silicates have been identified with Mg isotopes more in line with the mixing calculations (Nguyen and Messenger, 2014), lending support to a nova origin. A fundamental difficulty with this scenario is the lack of an explanation for the required mixing with solar material. Nittler et al. (2008) suggested that mass transfer between members of a stellar binary system, for example, nova ejecta reaccreted onto a companion (Marks et al., 1997) or AGB ejecta deposited onto a main sequence companion could explain the isotopic compositions of Group 1x grains. Clearly, additional isotopic data and modeling are needed to resolve the origins of these enigmatic grains.

5.7 Origins of ^{54}Cr-rich presolar oxide grains

The stellar synthesis of ^{54}Cr requires higher density of neutrons than achieved in the He shell of an AGB star, but models of certain shells of Type II supernovae (e.g., Rauscher et al., 2002), high-density Type 1a supernovae (Woosley, 1997), and electron-capture supernovae (ECSN; Wanajo et al., 2013) show that all can produce ^{54}Cr. When highly ^{54}Cr-rich nano-oxides were discovered around 2010 (Dauphas et al., 2010; Qin et al., 2011), it was thus immediately recognized that they must originate in supernovae, but the data could not distinguish which type. However, the discovery of extremely ^{54}Cr-rich grains, e.g., with $^{54}Cr/^{52}Cr > 10\times$ Solar (Fig. 8; Nittler et al., 2018), allows for better constraints on their origins. In particular, the thermonuclear ECSN model of Jones et al. (2019) was found to be an almost perfect match to the most ^{54}Cr-rich grain, 2–37 (Fig. 8), especially if the observed excess at mass 50 is attributed to ^{50}Ti (Fig. 8c), which is also synthesized in very high abundance in neutron-rich environments. Therefore, ECSN are likely to have been the sources of grain 2–37 and the other ^{54}Cr- and ^{50}Ti-rich nano-oxide grains, and the grains thus are potentially powerful probes of these still enigmatic astrophysical phenomena.

6 Structure and compositions of presolar oxide grains

Whereas the isotopic compositions of presolar grains reflect the nucleosynthesis of their progenitor stars, the crystal structures and elemental compositions of the grains record the condensation conditions and subsequent processing histories. Astrophysical condensation environment parameters, such as the ambient gas composition, pressure and temperature, and rate of cooling, are recorded in the individual grain elemental composition and structure. Post-condensation processing events, such as collisional processing or irradiation in the interstellar medium or solar nebula, as well as thermal and aqueous alteration on the host asteroid parent body, can impart interpretable signatures on the grain structure and/or composition. Fortunately, the refractory nature of oxides, such as corundum and other alumina phases, hibonite, and spinel, means that they are mostly unaffected by parent body alteration under the conditions experienced by most carbonaceous and unequilibrated ordinary chondrites. As a result of this resistance to parent body alteration, the structural and compositional features of presolar oxides can be interpreted to first order as faithfully recording primary condensation conditions, in some cases overprinted by processing in the interstellar medium. Refractory oxides are also resistant to radiation damage; individual displaced atoms remain as interstitial point defects in the lattice, rather than form extended damage tracks, and radiation-induced amorphization requires a very high dose. In contrast, presolar silicate phases are less refractory and more prone to loss of the primary condensation features due to subsequent thermal, aqueous, mechanical, and radiation processing. Whereas there is little correlation of presolar oxide abundances with petrographic grade of host, the observed abundance of presolar silicates (Floss and Haenecour, 2016) is significantly anti-correlated with the severity of hydrothermal alteration on the parent body. More information on the structural analysis of presolar silicates is available in Chapter 6.

Direct astrophysical observations of oxide dust in circumstellar environments provide important but limited constraints on the condensation conditions. Oxide dust grain formation in outflows from Asymptotic Giant Branch (AGB) stars and type II supernovae has been observed with infrared (IR) spectroscopy (Sloan et al., 1996; Posch et al., 1999; Rho et al., 2008). The details of IR spectral features depend on the crystal structure, grain size and shape, and elemental composition. The circumstellar spectra are fitted using models and reference spectra obtained from synthetic analog grains. Thus, measurements of the features of presolar stardust can help validate the circumstellar dust phase detection and inform the choices of reference spectra and modeling parameters. However, astronomical observations of oxide stardust grains face several challenges, such as the need for warm grains to provide significant emission at a low enough dust density to limit the disk opacity, and the overall lower abundance of Al, Ca, and Ti atoms to form dust compared to Si atoms in stellar envelopes. So far, in addition to amorphous and crystalline silicates,

astronomical detection of three oxides, Al_2O_3 (in crystalline and amorphous forms), $MgAl_2O_4$, and MgO, have been reported. The recent launch of the James Webb Space Telescope may lead to more detailed astronomical observations of the known phases and also provides increased sensitivity needed to measure less abundant phases, such as hibonite. However, coordinated secondary ion mass spectrometry-transmission electron microscopy (SIMS-TEM) studies will likely always be the sole means of probing certain stellar condensation processes for the smallest grains (few nm phases identified as subgrains of the primary presolar grain), rare grains that constitute <10% of the dust fraction, and the complex, heterogenous grains without any synthetic analogs for reference spectra.

In order to carry out the coordinated SIMS-TEM studies of presolar oxide grains, either as grain separates or in situ in the meteorite matrix, the use of a focused ion beam (FIB) workstation to extract an electron transparent section of individual grains identified by SIMS for the TEM analysis is essential. Early SIMS studies of oxide grains were performed on grain separates, extracted from the host meteorite using a series of acid dissolution steps, followed by centrifugation to extract grains of well-constrained density, specific to specific phases. The grain separates were then deposited onto Au foils to make mounts for SIMS, and on which oxygen isotope mapping was carried out to identify the ~1/300 Al_2O_3 grains with a nonsolar O isotope composition. The typical grain sizes (Fig. 4) for the Al_2O_3 and hibonite ($CaAl_{12}O_{19}$) grains range from sub-μm to few μm, and spinels are ~300 nm, which are too small for particle picking under an optical microscope but well suited to processing with the Ga^+ FIB. The smaller beam spot of the nanoSIMS compared to earlier SIMS instruments enabled the identification of more presolar oxide grains in situ. Extraction of the electron transparent section of these grains using FIB lift-out methods preserves the surrounding matrix material so that the petrographic context of grains in the host meteorite can also be studied by TEM.

Once the stardust grains are isotopically identified with SIMS, sectioned with FIB, and structurally and compositionally characterized with TEM, the primary guide for relating the grain properties to astrophysical condensation conditions comes from equilibrium condensation models (Chapter 12, Ebel, 2006). These models predict the order of condensation of the major dust phases from the highest temperature to the lowest for a given gas composition and pressure. For a gas of Solar composition, the sequence is corundum (α-Al_2O_3), followed by hibonite ($CaAl_{12}O_{19}$), perovskite ($CaTiO_3$), gehlenite ($Ca_2Al(Al,Si)O_7$), and spinel ($MgAl_2O_4$) (Table 3). Iron metal alloy, containing Ni, Cr, and other minor and trace metals, is predicted rather than oxide, followed by olivine (Mg_2SiO_4). In general, thermodynamic modeling parameters must be extrapolated to the relevant range of circumstellar conditions and are calculated for the most stable bulk phase at the relevant temperature. For Al_2O_3, corundum is used, although there are at least eight metastable polymorphs, in addition to amorphous Al_2O_3, that are readily synthesized experimentally (Levin and Brandon, 1998). Minor oxide phases, more refractory than corundum, such as ZrO_2 and TiO_2, are also possible condensates, but are not often discussed in the calculations regarding presolar grains, due to the low ex-

TABLE 3 Equilibrium condensation sequence for a gas of solar system composition at 0.1 mbar.

$T_{condensation}$ (K)	Formula	Phase
1764	ZrO_2	Zirconia
~1700	**TiO_2**	Rutile → anatase
1677	**Al_2O_3**	**Corundum, amorphous, γ, χ**
1659	**$CaAl_{12}O_{19}$**	**Hibonite**
1529	$Ca_2Al_2SiO_7$	Gehlenite
1441	$CaTiO_3$	Perovskite
1397	**$AlMg_2O_4$**	**Spinel**
1357	Fe	Fe alloy
1354	**Mg_2SiO_4**	**Forsterite**
1316	**$MgSiO_3$**	**Enstatite**
371	**Fe_3O_4**	**Magnetite**

Isotopic measurements confirm the existence of presolar dust grains of nominal elemental compositions listed in bold. Electron diffraction measurements confirm the minerals and metastable phases identifications of the phases listed in bold. Condensation temperatures taken from Lodders (2003) *except for TiO_2, for which an estimate is shown.*

pected abundance and size. Condensation kinetics, particularly the availability of seed molecules to act as nuclei, also plays a crucial role in grain formation, leading to condensation of metastable phases. Another important consideration is the residence time of the stardust grains in their progenitor stars before transport into the interstellar medium. The equilibrium condensation models indicate that hibonite forms by reaction of Ca from the gas with corundum dust grains and that continued cooling of the gas leads to formation of gehlenite by reaction of Si with hibonite dust. If no dust escaped the progenitor star at each stage, only the end products of the condensation sequence would be observed in the meteoritic record, but this is not the case; both corundum and hibonite are among the known presolar oxide phases.

6.1 Al_2O_3 grains

Structural data from TEM (Stroud et al., 2004, 2007; Takigawa et al., 2014a,c, 2018) and/or EBSD studies (Takigawa et al., 2014b) of 15 presolar Al_2O_3 grains have been reported (Table 4). Of the six grains for which TEM data has been reported, four have the corundum (α-Al_2O_3) thermodynamic equilibrium crystal structure, one is amorphous, and one is consistent with the metastable hexagonal polytype family (Levin and Brandon, 1998). The remaining nine grains, for which the crystal structure determination depends on electron backscatter diffraction (EBSD) analysis, include two identified as weakly crystalline or amorphous grains,

TABLE 4 Summary of structural and compositional data for Al_2O_3 grains.

Sample	Group	Phase	Size (μm)	Notes from TEM and/or EBSD studies
QUE060[1]	2	α	1.4 × 1.4	TEM and EBSD: faceted, polycrystalline, internal voids heterogeneous Mg, possible shock, possible impact crater
T96[2]	1	Amor.	1.2 × 0.7	TEM: stoichiometric Al_2O_3
T103[2]	1	α	1.0 × 0.5	TEM: 0.1 wt% Ti
Bishunpur 60–35[3]	1	α	1.3 × 0.8	EBSD: irregular; TEM: Ti oxide subgrain
Bishunpur 60–44[3]	1	α	1.5 × 0.8	TEM and EBSD: irregular, rough, polycrystalline α-Al_2O_3
RC075 58–09[3]	3	No ID	1.2 × 1.1	EBSD: faceted, rough, low crystallinity
RC075 58–33[3]	1	α	1.0 × 0.5	EBSD: faceted single crystal
RC075 58–49[3]	3	α	1.4 × 0.6	TEM and EBSD: irregular, rough
RC075 59–07[3]	1	α	1.7 × 1.5	TEM and EBSD: irregular, single crystal by EBSD, 2 or more grains by dark-field TEM, internal voids
RC075 59–08[3]	1	α	1.3 × 1.0	EBSD: irregular, low crystallinity; TEM: strained single crystal
RC075 59–09[3]	1	α or κ	1.7 × 1.3	EBSD: faceted single crystal α; TEM: possible κ
RC075 59–22[3]	1	α or κ	0.9 × 0.8	EBSD: faceted, rough, single crystal α; TEM: single crystal, possibly κ
Org-114–12[4]	2	Hex.	1.5 × 0.5	TEM: diffraction consistent with transitional alumina of hexagonal family (PDF 021–0010) 95 wt% Al_2O_3, 3.6 wt% MgO, 1.3 wt% TiO_2, possible impact crater
QUE053[5]	1	α	<0.5	TEM and EBSD: rounded single crystal
QUE067[5]	4	α	0.2 × 0.2	TEM: single crystal

[1]Takigawa et al. (2018), [2]Stroud et al. (2004), [3] Takigawa et al. (2014b,c), [4] Stroud et al. (2007), *and* [5]Takigawa et al. (2014a). *Grain name indicates meteorite in which it was found: QUE = Queen Alexandra Range 97,008; T = Tieschitz; RC075 = Roosevelt County 075; Org = Orgueil.*

one polycrystalline corundum grain, and six corundum single crystals. The grain shapes are generally rounded, some irregular and some with hints of faceting and equiaxed (Fig. 15), i.e., no grains with platy or rod microstructures have been ob-

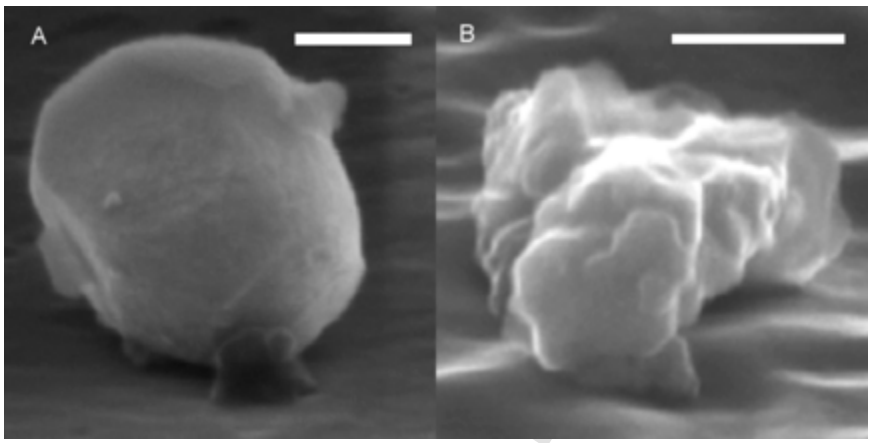

FIG. 15

Secondary electron images of presolar alumina, as extracted from the host meteorites by acid dissolution prior to isotopic measurements. Scale bars are 0.5 μm. (A) RC075 59–09. (B) Bishunpur 60–44. Grains vary in shape from faceted euhedral grains to rough, irregularly shaped grains.

- Adapted from Takigawa, A., Stroud, R.M., Nittler, L.R., Vicenzi, E.P., Herzing, A., Alexander, C.M.O'D., Huss, G.R., 2014a. Crystal structure, morphology, and isotopic compositions of presolar Al2O3 grains in unequilibrated ordinary chondrites. Lunar Planet. Sci. 45, abstract 1465; Takigawa, A., Tachibana, S., Huss, G.R., Nagashima, K., Makide, K., Krot, A.N., Nagahara, H., 2014b. Morphology and crystal structures of solar and presolar Al2O3 in unequilibrated ordinary chondrites. Geochim. Cosmochim. Acta 124, 309–327; Takigawa, A., Stroud, R.M., Nittler, L.R., Alexander, C.M.O'D., 2014c. A titanium oxide grain within a presolar corundum. Meteorit. Planet. Sci. 49, abstract #5389.

served. The mean grain size is ~1 μm, with a range ~0.5–2 μm, and aspect ratios of longest/shortest dimension <3.

All 15 of the TEM and EBSD analyzed alumina grains were studied ex situ, after isolation from the host meteorites as acid-resistant density separates from the matrices of chondritic meteorites. The preparation of the grain separates enables faster isotopic identification of the rare circumstellar alumina grains, which are outnumbered by solar system-formed corundum by ~300×, which in turn is a minor matrix mineral. Although corundum is extremely acid-resistant when well crystallized, amorphous alumina and other metastable polymorphs are more susceptible to etching (Takigawa et al., 2014b). In particular, Takigawa et al. (2014b) showed that surfaces subjected to ion irradiation were removed by subsequent exposure to the acid dissolution protocols used to prepare the alumina grain separates. In addition, sol–gel prepared amorphous alumina and metastable aluminas, produced by heating hydrated alumina, also dissolved in these acids. This suggests that the record of presolar alumina grains' exposure histories in the solar system and primordial interstellar medium, in the form of radiation-induced surface defects, if present, would be lost during laboratory processing. In order to investigate this possibility, SIMS

mapping to identify the presolar alumina in situ, followed by FIB lift-out of the grains that preserve the grain-matrix interfaces, will be necessary in the future.

Two of the ex situ grain cross sections do show evidence for possible grain-grain collisions in the interstellar medium, in the form of rounded pits at the grain surfaces. One of these grains, QUE060 (Takigawa et al., 2018), is corundum, with well-formed R-plane facets on four sides, and a ~0.3-μm deep cavity on one side. The crystal lattice planes show a ~0.3° rotational deviation across the grain, around the cavity. Grain QUE060 also shows heterogeneously distributed Mg, in domains <100 nm across that form a superstructure aligned with the host corundum lattice. The Mg is nearly pure ^{26}Mg, formed in situ in the grain by decay of ^{26}Al, with an average relative abundance of Mg/Al of 0.014, as measured by STEM-EDS. The clumping of the Mg indicates that the grain experienced a transient heating event, after the $^{26}\text{Al} \rightarrow {}^{26}\text{Mg}$ transformation. No specific signs of local amorphization, high crystal defect densities at the edges of the cavity, or any residue from impacting grains were retained in the grain cross section, but these may have been removed during the grain separation production.

Similar to QUE060, Orgueil 114–12 (Fig. 16; Stroud et al., 2007) shows a rounded cavity in an otherwise flat grain face, which suggests hypervelocity impact damage. Electron diffraction patterns obtained from the grain indicate that it is inconsistent with indexing to corundum, and it has been tentatively assigned to two or more crystallites of metastable alumina. The element composition of 114–12 is also unusual in that it is enriched in both Mg (3.6 wt% MgO) and Ti (1.3 wt% TiO_2). Group 2 grain 114–12 has the highest inferred $^{26}\text{Al}/^{27}\text{Al}$ ratio of any measured presolar oxide grain (Fig. 6d), so most of the measured high Mg content is certainly radiogenic ^{26}Mg, but a small ^{25}Mg enrichment indicates that it contains in-

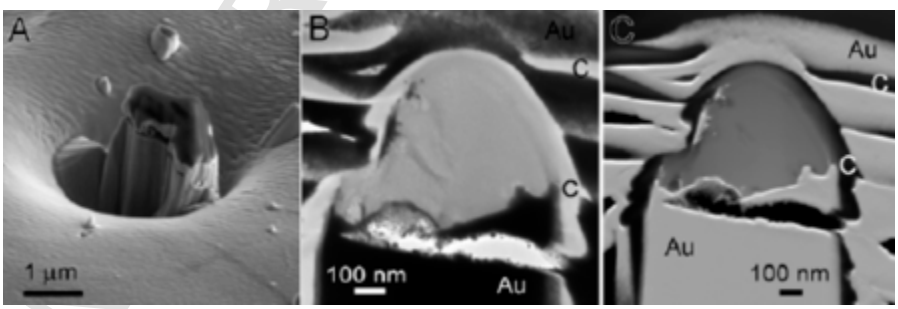

FIG. 16

(A) Secondary electron image of presolar Al_2O_3 grain 114–12 after isotopic measurement (Stroud et al., 2007). The grain is sitting on an Au substrate and surrounded by FIB-deposited C and redeposited Au. Bright-field (B) and dark-field (C) scanning transmission electron microscopy (STEM) images of a focused ion beam cross section of grain 114–12, revealing a possible impact crater in the lower left edge of the grain.

trinsic Mg as well. No subgrains or spatial compositional heterogeneities were observed; however, a *y*-shaped void was present in the center of the grain.

Subgrains, formed either as precondensed nucleation seeds, or exsolution precipitates appear to be relatively rare in presolar alumina. A TEM study of 15 presolar Al_2O_3 grains found only a single TiO_2 subgrain in one of them (Takigawa et al., 2014c).

6.2 Hibonite grains

Most equilibrium thermodynamic calculations predict hibonite ($CaAl_{12}O_{19}$) to be the second major oxide phase to condense from a gas of solar composition, through gas-grain reaction of Ca with corundum dust. In our solar system, hibonite is an important component of the earliest condensed solids, i.e., calcium, aluminum-rich inclusions found in chondritic meteorites. Meteoritic hibonite occurs as micrometer size platy grains, with substitutional Ti, Fe, V, and minor Si. The existence of presolar Al_2O_3 indicates that some corundum grains can escape the circumstellar envelopes prior to the ambient gas cooling to temperatures at which back-reaction initiates the transformation to hibonite.

TEM analysis (Table 5) of five presolar hibonite grains (KH1, KH2, KH6, KH15, KH21) isolated from the Krymka (LL3) OC meteorite (Stroud et al., 2008; Zega et al., 2011) and two grains analyzed in situ in the matrices of the Northwest Africa 582 CR3 chondrite (Leitner et al., 2012) and of the Acfer 094 ungrouped C-chondrite (Vollmer et al., 2013) are consistent with circumstellar-formed hibonite ($P6_3/mmc$, $a = 0.556$ nm, $c = 2.19$ nm). With the exception of the Acfer 094 grain, all presolar hibonites were large enough, i.e., ranging from submicron to a few micrometers in size, for the use of selected area electron diffraction to confirm the crystal phase. The grain shapes were platy (KH6, KH21, KH15, KH2) to needle-shaped (KH1), with some grains consisting of multiple connected plates (KH2 and KH15), and one irregular-shaped (NWA 6_8). In contrast, the Acfer 094 hibonite was identified as a collection of subgrains enriched in Ca and Al contained in a larger, amorphous presolar silicate, with the hibonite phase determination based on the presence of 1.1 nm lattice fringes in the most distinct 20-nm, Ca, Al-rich crystallite. Only one compositionally distinct subgrain was detected in the 7 hibonites. Grain NWA 6_8 also had a Ti-rich subgrain with Ca/Ti ~ 1 that was presumed to be perovskite ($CaTiO_3$), although a precise composition and definitive phase identification could not be made due to the small size (100 nm) of the subgrain.

The Krymka hibonites were all single crystals, with small orientation changes across the grain in the case of the grains consisting of connected plates. The Group 4 supernova grain KH2 (Figs. 14 and 17) did not differ significantly in its microstructure compared to the other (AGB-derived) grains. This is in contrast to presolar SiC, where notable differences in microstructures are observed between supernova and AGB star grains (Chapter 2). No evidence for tracks from charged particle irradiation has been observed, but regions of higher lattice defect concentrations within the grains, including stacking faults, were observed. The higher de-

TABLE 5 Summary of structural and compositional data for hibonite ($CaAl_{12}O_{19}$) grains.

Sample	Group	Size (μm)	Notes from TEM studies
32_03[1]	1	0.02	Identified as subgrains in amorphous silicate, based on lattice fringe spacing and EDS composition
KH1[2]	2	1.3 × 0.13 ± 0.08	Single crystal with stacking disorder on one edge $Ca_{1.04}Al_{11.58}Si_{0.09}Mg_{0.14}Ti_{0.11}Fe_{0.06}O_{19}$
KH2[2,3]	4	0.6 × 0.23	Single crystals with crack or gap $Ca_{0.98}Al_{11.77}Si_{0.02}Mg_{0.14}Ti_{0.09}Fe_{0.01}O_{19}$
KH6[2]	1	0.15 × 0.3	Single crystal with some stacking disorder $CaAl_{12}O_{19}$
KH15[2]	2	2.5 × 0.24 ± 0.12	Platy with zig-zag microstructure, $Ca_{0.98}Al_{11.77}Si_{0.02}Mg_{0.14}Ti_{0.09}Fe_{0.01}O_{19}$
KH21[2]	1	3.7 × 0.5 ± 0.2	Single crystal with stacking disorder on one end $Ca_{1.01}Al_{11.73}Mg_{0.21}Ti_{0.07}Si_{0.01}Fe_{0.01}O_{19}$ (grain average); lower in Ca and Mg and higher in Al in region of stacking disorder
6_8[4]	1	1.75 × 0.3	Contains 100 nm subgrain of possible perovskite

[1]Vollmer et al. (2013), *grain from Acfer 094 meteorite;* [2]Zega et al. (2011), [3]Stroud et al. (2008), *grains from Krymka meteorite; and* [4]Leitner et al. (2012), *grain from Northwest Africa 852 meteorite.*

fect density regions appeared to be correlated with higher concentrations of minor elements, e.g., Ti, and could be primary growth features given that stacking faults are common in hibonites in general. However, the highly defective areas were typically at the edge of the individual grains, rather than distributed homogenously, and could result from physical fracture of grains that consisted of multiple plates (see Zega et al., 2011, Fig. 4). The survival of multiple connected plates (KH15) through the ISM and accretion onto the Krymka parent body is somewhat surprising. If this survival was facilitated by an overgrowth of circumstellar silicate or interstellar organic matter, such material was lost in the acid dissolution process used to isolate the grain. The platy growth habit of these hibonites is inconsistent with formation by back-reaction of equiaxed Al_2O_3 grains with Ca and O alone. Instead, these grains may have formed by reaction of smaller corundum grains where Al was not yet fully depleted from the gas, consistent with the ~20 K difference in condensation onset temperatures.

The NWA 6_8 grain studied in situ has an irregular, non-compact shape, though it is not obviously platy. The one published diffraction pattern from this grain indicates that at least two distinct hibonite crystallites are present at a small angular separation in lattice orientation. Leitner et al. (2012) reported difficulty in obtaining

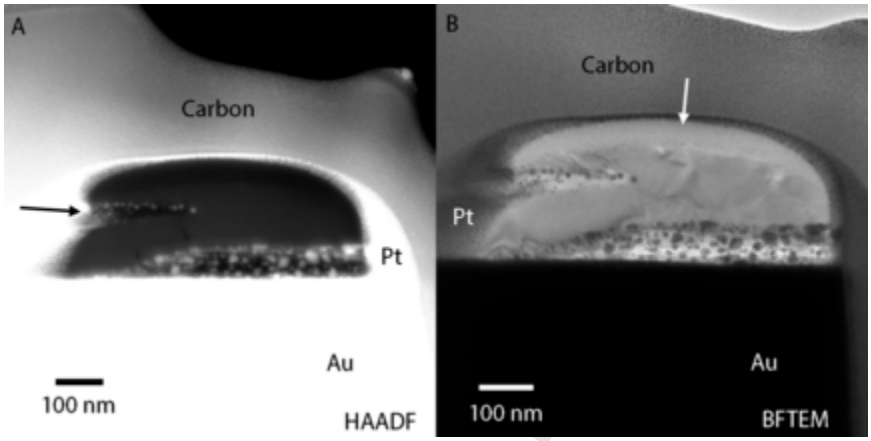

FIG. 17

High-angle annular dark-field STEM (A) and bright-field TEM (B) of presolar Group 4 hibonite grain KH2. The *black arrow* indicates a crack in the grain that could be due to impact fracturing (e.g., during a grain-grain collision event in the SN outflow, interstellar medium, or the solar nebula), or possibly is a primary feature of platy growth morphology. The *white arrow* indicates the SIMS-radiation damage layer where the grain is amorphous, below which diffraction contrast due to variations in strain in the lattice is visible. The strain supports the possibility of impact processing.

compositional data that did not include contributions of underlaying and neighboring grains in the FIB section, and thus the EDS elemental analysis shows significant contributions from Si, Mg, and Fe, in addition to Ca and Al. The reported relative uncertainty based on counting statistics in the elemental data is 100%, which presumably is an overestimate for the major elements Ca and Al. No other predicted condensate has Ca/Al within the uncertainty, so the phase identification is most likely correct.

A compositional trend among presolar oxides suggested by the TEM-EDS data from the Krymka grains is higher Ti contents in the Group 2 grains than in the Group 1 grains (Zega et al., 2011). This trend was confirmed with SIMS data estimates of the Ti/Al ratios of a larger population of grains, including alumina and hibonites. In general, the Ti content of the alumina grains is lower than that of hibonites, and lower in Group 1 grains of each phase than in Group 2 grains. The origin of this difference is possibly a difference in the condensation temperature histories of the grain condensation in the different stellar progenitors. Corundum and hibonite have very similar predicted condensation onset temperatures, with corundum ~20 K higher than hibonite for a given pressure and gas composition, i.e., 1665 and 1647 K for a gas of solar photospheric composition at 0.1 mbar, whereas Ti condensation is delayed until the initiation of perovskite at 1584 K. Thus, a higher Ti content in hibonite grains is consistent with the condensation of hibonite at the lower

temperature, closer to the onset of perovskite. As discussed above in Section 5.3, both Group 1 and 2 grains most likely formed in low- to intermediate-mass AGB stars, and thus differences in the relative Ti abundances in the circumstellar envelopes of the progenitor stars would not be expected. The higher Ti contents suggest that Group 2 oxides themselves may have formed at lower temperatures or pressures than Group 1 grains, but the underlying astrophysical reason for this is unclear.

6.3 Spinel

Spinel refers to $MgAl_2O_4$, the mineral, as well as the broader class of minerals with an AB_2O_4 stoichiometry and a cubic lattice structure. The lattice commonly takes the $Fd\bar{3}m$ (diamond) space group symmetry, with some variations, e.g., $F\bar{4}3m$, depending on cation occupancy and temperature. The two cations, A and B, in the prototypical spinel structure have +2 and +3 oxidation states, respectively. The naming convention for the spinels is according to the B cation, so that the Al spinel group includes spinel $MgAl_2O_4$, hercynite $FeAl_2O_4$, and the solid solution pleonaste $(Mg,Fe)Al_2O_4$; the Fe spinel group includes magnetite $FeFe_2O_4$, trevorite $NiFe_2O_4$, ulvopspinel $TiFe_2O_4$, and magnesioferrite $MgFe_2O_4$; and the Cr spinel group includes $FeCr_2O_4$ chromite and magnesiochromite $MgCr_2O_4$. In thermodynamic equilibrium models, the first to condense is Mg-Al spinel, by reaction of Mg from the gas with corundum (Al_2O_3) dust. Metals, including Fe, Ni, and Cr, are expected to condense into Fe alloys at temperatures within ~50 K below Mg-Al spinel, rather than be incorporated either into silicates or oxides; chromite condensation would occur at ~200 K below Mg-Al spinel, and magnetite at ~1000 K below Mg-spinel, if any Cr or Fe was available to condense.

The available TEM data (Table 6) for presolar spinels and related phases indicate that most, but not all, grains conform to the predictions of equilibrium condensation calculations. Of the 11 total grains for which TEM data are available, 8 are Mg-Al dominated, two are Fe dominated, and one is Fe-Cr. Even the Mg-Al dominated grains show incorporation of additional cation species, including Fe, Ni, Cr, and Ti. These minor element substitutions could reflect absorption of the less refractory species during the cooling of the gas in the primordial stellar outflow, kinetic constraints on the condensation, or incorporation of solar system material from the host meteorite. Of the eight Mg-Al spinel grains, four are single crystals: Adelaide 7a-1-o1, Murray 2-19-13, UOC-S1, UOC-S2 (Fig. 18; Zega et al., 2014, 2020), one is an aggregate of spinel grains: DOM-9 (Zega et al., 2020), one is polycrystalline: A2-2-15 (Nittler et al., 2020), and one is crystalline spinel with an amorphous silicate rim: W7027E6psg1 (Nguyen et al., 2022). An additional polycrystalline Mg-Al spinel with magnetite inclusions was reported as part of an oxide-silicate composite grain F2–8 (Singerling et al., 2023). Two of the grains are thought to be Fe oxides, one amorphous: 3_13b (Nguyen et al., 2016) and one a single crystal of magnetite: LAP-103 (Zega et al., 2015), which would require significant deviation from the expected condensation conditions of Group 1 grains

TABLE 6 Summary of structural and compositional data for spinel grains.

Sample	Group	Size (μm)	Notes from TEM studies
7a-1-o1[1]	1	0.4 × 0.3	Single crystal $(Mg_{0.69}Fe_{0.3})(Al_{1.98}Cr_{0.02})O_4$, possible Cr-rich alteration rim
DOM-9[1]	1	0.2 × 0.2	Five grain aggregate $(Mg_{1.1}Fe_{0.04})(Al_{1.65}Cr_{0.26})O_4$ in polycrystalline Mg-rich pyroxene
LAP-103[2]	1	0.75	Fe_3O_4 single crystal
ORG-36-21[3]	1	0.4 1.0 1.3 × 0.8	Three connected crystallites $(Fe_{0.67}Mg_{0.31}Ni_{0.02})(Cr_{1.58}Al_{0.21}Mg_{0.06}Ti_{0.13})O_4$, with Al-rich subgrains with coherent lattice
Murray 2-19-13[3]	2	0.33 × 0.52	Single crystal $(Mg_{0.97}Fe_{0.02})(Al_{1.74}Cr_{0.22}Si_{0.03})O_4$
UOC-S1[3]	1	0.17 × 0.4	Single crystal, sub-stoichiometric Mg/Al $(Mg_{0.68}Fe_{0.03}Ca_{0.01})(Al_{2.19}Cr_{0.01})O_4$
UOC-S2[3]	1	0.15 × 0.42	Single crystal with some stacking disorder $(Mg_{0.98}Fe_{0.01})(Al_{1.94}Cr_{0.06})0_4$
A2-2-15[4]	1	0.33	$MgAl_2O_4$ with minor chromium
W7027E6psg1[5]	1	0.35	$MgAl_2O_4$ with trace Ti and Fe surrounded by Mg-rich, non-stoichiometric, amorphous silicate in an interplanetary dust particle
3_13b[6]	1	0.2	Amorphous, Fe oxide ~$Fe_{0.24}O_{0.4}$
F2–8[7]	1	0.68 × 0.32	Composite grain consisting of a polycrystalline stoichiometric $MgAl_2O_4$ grain with magnetite subgrains, Mg-rich olivine and Ca-rich pyroxene

[1]Zega et al. (2020), *7a-1-o1 is from the Adelaide meteorite, DOM-9 from Dominion Range 08006;* [2]Zega et al. (2015), *grain from LaPaz Icefield 031117;* [3]Zega et al. (2014), *ORG-36-21 is from Orgueil and UOC grains are from a mixed residue of different ordinary chondrites;* [4]Nittler et al. (2020), *grain is from Dominion Range 08006;* [5]Nguyen et al. (2022), [6]Nguyen et al. (2016), *and* [7]Singerling et al. (2023), *grain is from Semarkona meteorite.*

from AGB stars of near solar mass and metallicity. The most unusual presolar spinel grain (ORG-36-21, Fig. 19) consists of three connected Cr-spinel crystallites with Al-rich spinel subgrains (Zega et al., 2014). The microstructure of this grain suggests formation in a rapidly cooling gas at the upper temperature range for chromite and a lower limit for Mg-Al spinel, leading to formation of the Al-rich subgrains by solid state precipitation as the grain cooled.

7 Summary and outlook

Since the discovery of the first presolar Al_2O_3 grain more than 30 years ago (Hutcheon et al., 1994), more than 3000 presolar oxides of various mineralogies

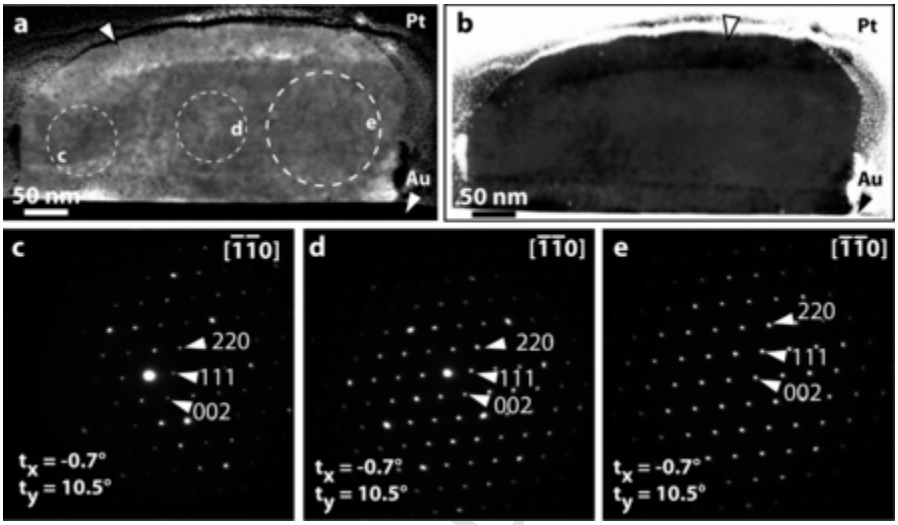

FIG. 18

Bright-field STEM (A), HAADF STEM (B), and selected area diffraction (C–E) of presolar spinel grain UOC-S2. The *white arrows* in (A) and (B) indicate the amorphous layer from the ion irradiation during SIMs measurements. The grain is a single crystal, oriented close to the [110] zones axis, but exhibits a slight change lattice orientation from light to right (C–E), as indicated by the diffraction patterns acquired at the same stage tilt (t_x,t_y). The Au is the SIMS mount, and Pt is the protective mask deposited during the FIB sample preparation.

- Adapted from Zega, T.J., Nittler, L.R., Gyngard, F., Alexander, C.M.O'D., Stroud, R.M., Zinner, E.K., 2014. A transmission electron microscopy study of presolar spinel. Geochim. Cosmochim. Acta 124, 152–169.

have been identified in meteorites, interplanetary dust particles, and even the recently returned samples from asteroid Ryugu (Barosch et al., 2022b). A detailed consideration of their isotopic systematics indicates that a large majority of the grains (^{17}O-rich and solar-to-depleted ^{18}O) originated in the winds of low- to intermediate-mass Asymptotic Giant Branch (AGB) stars. A much smaller fraction (<10%) of the grains are ^{18}O-rich and likely formed in type II supernovae. The origins of some grains are more ambiguous, though classical novae are likely suspects for the most ^{17}O-enriched grains. Comparisons of the grain isotope data with astrophysical models of GCE and stellar nucleosynthesis generally find broad agreement, but there are important exceptions. For example, Mg, Ca, and Ti isotopes are all expected to reflect GCE, but show more scatter than expected, perhaps indicating a high degree of inhomogeneity in the chemical evolution of the Galaxy. The observation that most supernova oxides are ^{18}O-rich when supernova-II ejecta is dominated by ^{16}O remains unexplained, but may be related to grain size bias in the extant presolar grain database and/or destruction of ^{16}O-rich grains by reverse shocks in supernova ejecta. The physical origin of the deep mixing in AGB stars in-

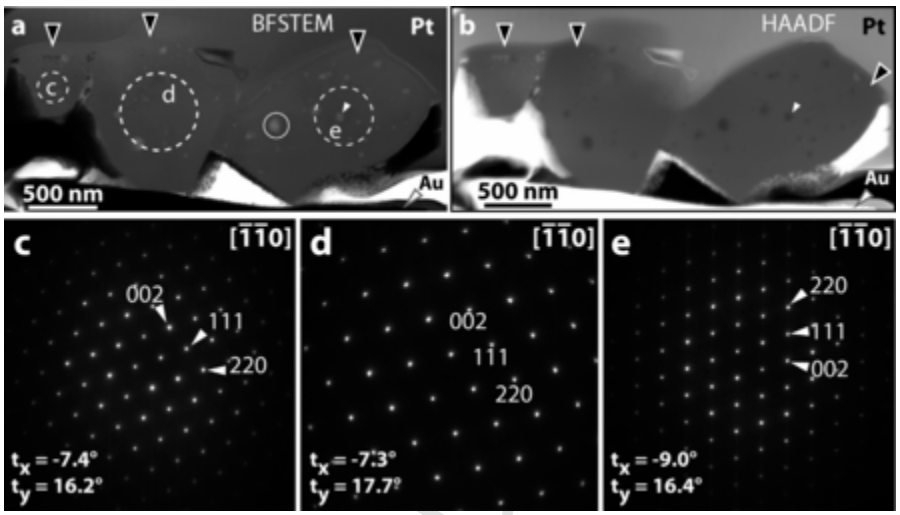

FIG. 19

(A) Bright-field STEM image, (B) HAADF STEM image, (C–E) selected area diffraction patterns acquired from areas outlined by the labeled circles shown in (A) of presolar spinel ORG-36-21. The grain contains three connected crystallites (A, B *black arrowheads with white outline*). Subgrains, which appear bright in the bright-field-STEM image and dark in the HAADF image (A, B *white arrowheads*), occur throughout each of the spinel crystals. The Au is the SIMS mount, and Pt is the protective mask deposited during the FIB sample preparation.

- Adapted from Zega, T.J., Nittler, L.R., Gyngard, F., Alexander, C.M.O'D., Stroud, R.M., Zinner, E.K., 2014. A transmission electron microscopy study of presolar spinel. Geochim. Cosmochim. Acta 124, 152–169.

dicated by Group 2 grains remains inadequately explained. For most elements besides O, Mg, and Al, there remains relatively little isotopic data for presolar oxide grains, but multielement data is the most valuable for inferring the origins of presolar grains and using them to constrain astrophysical models.

Detailed transmission electron microscopy studies are limited to a few grains of the major presolar oxide phases: 15 Al_2O_3, 7 hibonites, and 11 spinels, and mostly from the Group 1–3 classification of grains indicating an origin in low-to-intermediate mass AGB stars, with only one Group 4 Al_2O_3 and one Group 4 hibonite from type II supernovae. Among these grains, there is significant diversity in microstructure and minor element compositions consistent with variations in both condensation conditions and subsequent processing, but none of the grains has a fluffy aggregate structure often used to model interstellar grains. The Al_2O_3 grains vary in shape from euhedral, faceted single crystals to rough, elongated, and irregular and include a few grains with a metastable crystal structure, in addition to the predominant, stale corundum phase. Hibonite grains are commonly platy, with some single plates and some containing multiple connected plates. The spinel grains show the greatest variation in cation chemistry, consistent with the ability of the spinel lattice

structure to accommodate a wide range of elements. It is not yet known whether the minor elements in these spinel grains were incorporated during condensation, or are due to thermal or aqueous processing on the asteroid parent body. Subgrains in the spinels appear to have formed by solid state precipitation during cooling of the grains. There is no clear evidence for radiation processing of the grains, but such signatures might be lost during the acid-dissolution processing used to concentrate them for isotopic measurements. More in situ analyses are needed to look for nebular and interstellar medium processing. The probable evidence for collisional processing prior to the grains' incorporation on the host asteroids is recorded as likely impact craters in two Al_2O_3 grains and as concentrated lattice defects and fractured grain faces in at least two hibonites. The variations in shape, composition, and elemental compositions could significantly affect the optical properties of the grains in the infrared and complicate the spectral identification of dust in stellar outflows. In the coming decades, advances in the ability to measure infrared absorption properties at the nanoscale, using monochromated electron energy loss spectroscopy (Stroud et al., 2018) and other methods, could provide direct measurements of the optical properties of real stardust in the laboratory for use as reference spectra in interpreting the circumstellar spectra. Improvements in spatial resolution and collection efficiency of the SIMS measurements in the next decade might enable isotopic measurements of more subgrains of large grains observed by TEM, for better constraints on dust formation processes in different stellar environments.

References

Alexander, C.M.O'D., Nittler, L.R., 1999. The galactic chemical evolution of Si, Ti and O isotopes. Astrophys. J. 519, 222–235.

Amari, S., Anders, E., Virag, A., Zinner, E., 1990. Interstellar graphite in meteorites. Nature 345, 238–240.

Amari, S., Zinner, E., Lewis, R.S., 1996. ^{41}Ca in presolar graphite of supernova origin. Astrophys. J. 470, L101–L104.

Asplund, M., Amarsi, A.M., Grevesse, N., 2021. The chemical make-up of the sun: A 2020 vision. Astron. Astrophys. 653, A141.

Barosch, J., Nittler, L.R., Wang, J., Dobrică, E., Brearley, A.J., Hezel, D.C., Alexander, C.M.O.'.D., 2022a. Presolar O- and C-anomalous grains in unequilibrated ordinary chondrite matrices. Geochim. Cosmochim. Acta 335, 169–182.

Barosch, J., Nittler, L.R., Wang, J., Alexander, C.M.O.'.D., De Gregorio, B.T., Engrand, C., Kebukawa, Y., Nagashima, K., Stroud, R.M., Yabuta, H., Abe, Y., Aléon, J., Amari, S., Amelin, Y., Bajo, K.-i., Bejach, L., Bizzarro, M., Bonal, L., Bouvier, A., Carlson, R.W., Chaussidon, M., Choi, B.-G., Cody, G.D., Dartois, E., Dauphas, N., Davis, A.M., Dazzi, A., Deniset-Besseau, A., Di Rocco, T., Duprat, J., Fujiya, W., Fukai, R., Gautam, I., Haba, M.K., Hashiguchi, M., Hibiya, Y., Hidaka, H., Homma, H., Hoppe, P., Huss, G.R., Ichida, K., Iizuka, T., Ireland, T.R., Ishikawa, A., Ito, M., Itoh, S., Kamide, K., Kawasaki, N., Kilcoyne, D., Kita, N.T., Kitajima, K., Kleine, T., Komatani, S., Komatsu, M., Krot, A.N., Liu, M.-C., Martins, Z., Masuda, Y., Mathurin, J., McKeegan, K.D., Montagnac, G., Morita, M., Mostefaoui, S., Motomura, K., Moynier, F., Nakai, I., Nguyen, A.N., Ohigashi, T., Okumura, T., Onose, M., Pack, A., Park, C., Piani, L., Qin, L., Quirico, E., Remusat, L., Russell, S.S., Sakamoto, N., Sandford, S.A., Schönbächler, M., Shigenaka,

M., Suga, H., Tafla, L., Takahashi, Y., Takeichi, Y., Tamenori, Y., Tang, H., Terada, K., Terada, Y., Usui, T., Verdier-Paoletti, M., Wada, S., Wadhwa, M., Wakabayashi, D., Walker, R.J., Yamashita, K., Yamashita, S., Yin, Q.-Z., Yokoyama, T., Yoneda, S., Young, E.D., Yui, H., Zhang, A.-C., Abe, M., Miyazaki, A., Nakato, A., Nakazawa, S., Nishimura, M., Okada, T., Saiki, T., Tanaka, S., Terui, F., Tsuda, Y., Watanabe, S.-i., Yada, T., Yogata, K., Yoshikawa, M., Nakamura, T., Naraoka, H., Noguchi, T., Okazaki, R., Sakamoto, K., Tachibana, S., Yurimoto, H., 2022b. Presolar stardust in asteroid Ryugu. Astrophys. J. 935, L3.

Bernatowicz, T., Fraundorf, G., Tang, M., Anders, E., Wopenka, B., Zinner, E., Fraundorf, P., 1987. Evidence for interstellar SiC in the Murray carbonaceous meteorite. Nature 330, 728–730.

Bertoldi, F., Carilli, C.L., Cox, P., Fan, X., Strauss, M.A., Beelen, A., Omont, A., Zylka, R., 2003. Dust emission from the most distant quasars. Astron. Astrophys. 406, L55–L58.

Boothroyd, A.I., Sackmann, I.-J., 1999. The CNO-isotopes: deep circulation in red giants and first and second dredge-up. Astrophys. J. 510, 232–250.

Boothroyd, A.I., Sackmann, I.-J., Wasserburg, G.J., 1994. Predictions of oxygen isotope ratios in stars and of oxygen-rich interstellar grains in meteorites. Astrophys. J. 430, L77–L80.

Boothroyd, A.I., Sackmann, I.-J., Wasserburg, G.J., 1995. Hot bottom burning in stars and oxygen isotopic abundances. Astrophys. J. 442, L21–L24.

Choi, B.-G., Huss, G.R., Wasserburg, G.J., 1998. Presolar corundum and spinel in ordinary chondrites: origins from AGB stars and a supernova. Science 282, 1282–1289.

Choi, B.-G., Wasserburg, G.J., Huss, G.R., 1999. Circumstellar hibonite and corundum and nucleosynthesis in asymptotic giant branch stars. Astrophys. J. 522, L133–L136.

Clayton, D.D., 1988. Isotopic anomalies: chemical memory of galactic evolution. Astrophys. J. 334, 191–195.

Clayton, R.N., Grossman, L., Mayeda, T.K., 1973. A component of primitive nuclear composition in carbonaceous meteorites. Science 182, 485–488.

Clayton, D.D., Arnett, D., Kane, J., Meyer, B.S., 1997. Type X silicon carbide presolar grains: type Ia supernovae condensates? Astrophys. J. 486, 824–834.

Dauphas, N., Remusat, L., Chen, J.H., Roskosz, M., Papanastassiou, D.A., Stodolna, J., Guan, Y., Ma, C., Eiler, J.M., 2010. Neutron-rich chromium isotope anomalies in supernova nanoparticles. Astrophys. J. 720, 1577–1591.

De Looze, I., Barlow, M.J., Swinyard, B.M., Rho, J., Gomez, H.L., Matsuura, M., Wesson, R., 2017. The dust mass in Cassiopeia A from a spatially resolved Herschel analysis. Mon. Not. R. Astron. Soc. 465, 3309–3342.

Dearborn, D.S.P., 1992. Diagnostics of stellar evolution: the oxygen isotopes. Phys. Rep. 210, 367–382.

Ebel, D.S., 2006. Condensation of rocky material in astrophysical environments. In: Lauretta, D.S., McSween, H.Y., Jr. (Eds.), Meteorites and the Early Solar System II. University of Arizona Press, Tucson, pp. 253–277.

Floss, C., Haenecour, P., 2016. Presolar silicate grains: abundances, isotopic and elemental compositions, and the effects of secondary processing. Geochem. J. 50, 3–25.

Floss, C., Stadermann, F.J., Bose, M., 2008. Circumstellar Fe oxide from the Acfer 094 carbonaceous chondrite. Astrophys. J. 672, 1266–1271.

Gay, P.L., Lambert, D.L., 2000. The isotopic abundances of magnesium in stars. Astrophys. J. 533, 260–270.

Gehrz, R.D., 1989. Sources of stardust in the galaxy. In: Allamandola, L.J., Tielens, A.G.G.

(Eds.), Interstellar Dust. Kluwer Academic Publishers, Dordrecht, pp. 445–453.
Gyngard, F., Nittler, L.R., Zinner, E.K., Jose, J., 2010a. Oxygen-rich stardust grains from novae. Proc. 11th Symposium on Nuclei in the Cosmos. Heidelberg, Germany, Jul 19–23, PoS(NIC XI), 141.
Gyngard, F., Zinner, E., Nittler, L.R., Morgand, A., Stadermann, F.J., Hynes, K.M., 2010b. Automated NanoSIMS measurements of spinel stardust from the Murray meteorite. Astrophys. J. 717, 107–120.
Gyngard, F., Amari, S., Zinner, E., Marhas, K., 2018. Correlated silicon and titanium isotopic compositions of presolar SiC grains from the Murchison CM2 chondrite. Geochim. Cosmochim. Acta 221, 145–161.
Haenecour, P., Floss, C., Zega, T. J., Croat, T. K., Wang, A., Jolliff, B. L., Carpetner, P., 2018. Presolar silicates in the matrix and fine-grained rims around chondrules in primitive CO3.0 chondrites: Evidence for pre-accretionary aqueous alteration of the rims in the solar nebula. Geochim. Cosmichim. Acta 221, 379–405.
Harris, M.J., Lambert, D.L., 1984a. Oxygen isotopes in the atmospheres of Betelgeuse and Antares. Astrophys. J. 281, 739–745.
Harris, M.J., Lambert, D.L., 1984b. Oxygen isotopic abundances in the atmospheres of seven red giant stars. Astrophys. J. 285, 674–682.
Harris, M.J., Lambert, D.L., Smith, V.V., 1985. Oxygen isotopic abundances in evolved stars. I. Six barium stars. Astrophys. J. 292, 620–627.
Hoppe, P., Amari, S., Zinner, E., Ireland, T., Lewis, R.S., 1994. Carbon, nitrogen, magnesium, silicon, and titanium isotopic compositions of single interstellar silicon carbide grains from the Murchison carbonaceous chondrite. Astrophys. J. 430, 870–890.
Hoppe, P., Leitner, J., Kodolányi, J., 2015. New constraints on the abundances of silicate and oxide stardust from supernovae in the Acfer 094 meteorite. Astrophys. J. 808, L9.
Hoppe, P., Leitner, J., Kodolányi, J., 2018. New insights into the galactic chemical evolution of magnesium and silicon isotopes from studies of silicate stardust. Astrophys. J. 869, 47.
Hoppe, P., Leitner, J., Kodolányi, J., Vollmer, C., 2021. Isotope systematics of presolar silicate grains: new insights from magnesium and silicon. Astrophys. J. 913, 10.
Huss, G.R., Hutcheon, I.D., Wasserburg, G.J., Stone, J., 1992. Presolar (?) corundum in the Orgueil meteorite. Lunar Planet. Sci. XXIII, 563–564.
Huss, G.R., Fahey, A.J., Gallino, R., Wasserburg, G.J., 1994. Oxygen isotopes in circumstellar Al_2O_3 grains from meteorites and stellar nucleosynthesis. Astrophys. J. 430, L81–L84.
Hutcheon, I.D., Huss, G.R., Fahey, A.J., Wasserburg, G.J., 1994. Extreme ^{26}Mg and ^{17}O enrichments in an Orgueil corundum: identification of an interstellar oxide grain. Astrophys. J. 425, L97–L100.
Indebetouw, R., Matsuura, M., Dwek, E., Zanardo, G., Barlow, M.J., Baes, M., Bouchet, P., Burrows, D.N., Chevalier, R., Clayton, G.C., Fransson, C., Gaensler, B., Kirshner, R., Lakićević, M., Long, K.S., Lundqvist, P., Martí-Vidal, I., Marcaide, J., McCray, R., Meixner, M., Ng, C.-Y., Park, S., Sonneborn, G., Staveley-Smith, L., Vlahakis, C., van Loon, J., 2014. Dust production and particle acceleration in supernova 1987A revealed with ALMA. Astrophys. J. 782, L2.
Jadhav, M., Amari, S., Marhas, K.K., Zinner, E., Maruoka, T., Gallino, R., 2008. New stellar sources for high-density, presolar graphite grains. Astrophys. J. 682, 1479–1485.
Jones, S., Röpke, F.K., Fryer, C., Ruiter, A.J., Seitenzahl, I.R., Nittler, L.R., Ohlmann, S.T., Reifarth, R., Pignatari, M., Belczynski, K., 2019. Remnants and ejecta of thermonuclear electron-capture supernovae. Constraining oxygen-neon deflagrations in high-density

white dwarfs. Astron. Astrophys. 622, A74.
José, J., Hernanz, M., Amari, S., Lodders, K., Zinner, E., 2004. The imprint of nova nucleosynthesis in presolar grains. Astrophys. J. 612, 414–428.
Karakas, A.I., Lugaro, M., 2016. Stellar yields from metal-rich asymptotic giant branch models. Astrophys. J. 825, 26.
Kemper, F., Vriend, W.J., Tielens, A.G.G.M., 2004. The absence of crystalline silicates in the diffuse interstellar medium. Astrophys. J. 609, 826–837.
Kobayashi, C., Karakas, A.I., Umeda, H., 2011. The evolution of isotope ratios in the milky way galaxy. Mon. Not. R. Astron. Soc. 414, 3231–3250.
Lebzelter, T., Straniero, O., Hinkle, K.H., Nowotny, W., Aringer, B., 2015. Oxygen isotopic ratios in intermediate-mass red giants. Astron. Astrophys. 578, A33.
Leitner, J., Hoppe, P., 2019. A new population of dust from stellar explosions among meteoritic stardust. Nat. Astron. 3, 725–729.
Leitner, J., Vollmer, C., Hoppe, P., Zipfel, J., 2012. Characterization of presolar material in the CR chondrite Northwest Africa 852. Astrophys. J. 745, 38.
Leitner, J., Hoppe, P., Floss, C., Hillion, F., Henkel, T., 2018. Correlated nanoscale characterization of a unique complex oxygen-rich stardust grain: implications for circumstellar dust formation. Geochim. Cosmochim. Acta 221, 255–274.
Levin, I., Brandon, D., 1998. Metastable alumina polymorphs: crystal structures and transition sequences. J. Am. Ceram. Soc. 81, 1995–2012.
Lewis, R.S., Tang, M., Wacker, J.F., Anders, E., Steel, E., 1987. Interstellar diamonds in meteorites. Nature 326, 160–162.
Liu, M.-C., Chaussidon, M., Srinivasan, G., McKeegan, K.D., 2012. A lower initial abundance of short-lived ^{41}Ca in the early solar system and its implications for solar system formation. Astrophys. J. 761, 137.
Liu, N., Nittler, L.R., Pignatari, M., Alexander, C.M.O'D., Wang, J., 2017. Stellar origin of ^{15}N-rich presolar SiC grains of type AB: supernovae with explosive hydrogen burning. Astrophys. J. 841, L1.
Lodders, K., 2003. Solar system abundances and condensation temperatures of the elements. Astrophys. J. 591, 1220–1247.
Lugaro, M., Zinner, E., Gallino, R., Amari, S., 1999. Si isotopic ratios in mainstream presolar SiC grains revisited. Astrophys. J. 527, 369–394.
Lugaro, M., Karakas, A.I., Nittler, L.R., Alexander, C.M.O'D., Hoppe, P., Iliadis, C., Lattanzio, J.C., 2007. On the asymptotic giant branch star origin of peculiar spinel grain OC2. Astron. Astrophys. 461, 657–664.
Lugaro, M., Karakas, A.I., Bruno, C.G., Aliotta, M., Nittler, L.R., Bemmerer, D., Best, A., Boeltzig, A., Broggini, C., Caciolli, A., Cavanna, F., Ciani, G.F., Corvisiero, P., Davinson, T., Depalo, R., Di Leva, A., Elekes, Z., Ferraro, F., Formicola, A., Fülöp, Z., Gervino, G., Guglielmetti, A., Gustavino, C., Gyürky, G., Imbriani, G., Junker, M., Menegazzo, R., Mossa, V., Pantaleo, F.R., Piatti, D., Prati, P., Scott, D.A., Straniero, O., Strieder, F., Szücs, T., Takács, M.P., Trezzi, D., 2017. Origin of meteoritic stardust unveiled by a revised proton-capture rate of ^{17}O. Nat. Astron. 1, 0027.
Lugaro, M., Cseh, B., Vilagos, B., Karakas, A.I., Ventura, P., Dell'Agli, F., Trappitsch, R., Hampel, M., D'Orazi, V., Pereira, C.B., Tagliente, G., Szabo, G.M., Pignatari, M., Battino, U., Tattersall, A., Ek, M., Schoenbachler, M., Hron, J., Nittler, L.R., 2020. Origin of large meteoritic SiC stardust grains in metal-rich AGB stars. Astrophys. J. 898, 96.
Marks, P.B., Sarna, M.J., Prialnik, D., 1997. The chemical evolution of the secondary stars in close binary systems during nova outbursts. Mon. Not. R. Astron. Soc. 290, 283–291.

McKeegan, K.D., Kallio, A.P.A., Heber, V.S., Jarzebinski, G., Mao, P.H., Coath, C.D., Kunihiro, T., Wiens, R.C., Nordholt, J.E., Moses, R.W., Reisenfeld, D.B., Jurewicz, A.J.G., Burnett, D.S., 2011. The oxygen isotopic composition of the sun inferred from captured solar wind. Science 332, 1528–1532.

Meléndez, J., Cohen, J.G., 2007. Magnesium isotopes in metal-poor dwarfs: the rise of AGB stars and the formation timescale of the galactic halo. Astrophys. J. 659, L25–L28.

Messenger, S., Keller, L.P., Stadermann, F.J., Walker, R.M., Zinner, E., 2003. Samples of stars beyond the solar system: silicate grains in interplanetary dust. Science 300, 105–108.

Messenger, S., Keller, L.P., Lauretta, D.S., 2005. Supernova olivine from cometary dust. Science 309, 737–741.

Meyer, B.S., Weaver, T.A., Woosley, S.E., 1995. Isotope source table for a $25M_{\odot}$ supernova. Meteoritics 30, 325–334.

Meyer, B.S., Krishnan, T.D., Clayton, D.D., 1996. ^{48}Ca production in matter expanding from high temperature and density. Astrophys. J. 462, 825–838.

Nagashima, K., Krot, A.N., Yurimoto, H., 2004. Stardust silicates from primitive meteorites. Nature 428, 921–924.

Nguyen, A.N., Messenger, S., 2014. Resolving the stellar sources of isotopically rare presolar silicate grains through Mg and Fe isotopic analyses. Astrophys. J. 784, 149.

Nguyen, A.N., Zinner, E., 2004. Discovery of ancient silicate stardust in a meteorite. Science 303, 1496–1499.

Nguyen, A., Zinner, E., Lewis, R.S., 2003. Identification of small presolar spinel and corundum grains by isotopic raster imaging. Pub. Astron. Soc. Aust. 20, 382–388.

Nguyen, A.N., Stadermann, F.J., Zinner, E., Stroud, R.M., Alexander, C.M.O.'.D., Nittler, L.R., 2007. Characterization of presolar silicate and oxide grains in primitive carbonaceous chondrites. Astrophys. J. 656, 1223–1240.

Nguyen, A.N., Keller, L.P., Messenger, S., 2016. Mineralogy of presolar silicate and oxide grains of diverse stellar origins. Astrophys. J. 818, 51.

Nguyen, A.N., Nittler, L.R., Alexander, C.M.O.'.D., Hoppe, P., 2018. Titanium isotopic compositions of rare presolar SiC grain types from the Murchison meteorite. Geochim. Cosmochim. Acta 221, 162–181.

Nguyen, A.N., Nakamura-Messenger, K., Keller, L.P., Messenger, S., 2022. Diverse assemblage of presolar and solar system materials in anhydrous interplanetary dust particles: coordinated nanoSIMS and TEM analyses. Geochim. Cosmochim. Acta 336, 131–149.

Nichols, R.H., Jr., Ott, U., Kitts, K., Podosek, F.A., 2000. Chromium-54 isotopic anomaly distribution in Orgueil colloidal separates. Meteorit. Planet. Sci. Suppl. 35, A119.

Nittler, L.R., 2005. Constraints on heterogeneous galactic chemical evolution from meteoritic stardust. Astrophys. J. 618, 281–296.

Nittler, L.R., 2009. On the mass and metallicity distributions of the parent AGB stars of O-rich presolar stardust grains. Pub. Astron. Soc. Aust. 26, 271–277.

Nittler, L.R., Alexander, C.M.O'D., 2003. Automated isotopic measurements of micron-sized dust: application to meteoritic presolar silicon carbide. Geochim. Cosmochim. Acta 67, 4961–4980.

Nittler, L.R., Cowsik, R., 1997. Galactic age estimates from O-rich stardust in meteorites. Phys. Rev. Lett. 78, 175–178.

Nittler, L.R., Dauphas, N.D., 2006. Meteorites and the chemical evolution of the milky way. In: Lauretta, D.S., McSween, H.Y., Jr. (Eds.), Meteorites and the Early Solar System II.

University of Arizona Press, Tucson, pp. 127–146.
Nittler, L.R., Walker, R.M., Zinner, E., Hoppe, P., Lewis, R.S., 1993. Identification of an interstellar oxide grain from the Murchison meteorite by ion imaging. Lunar Planet. Sci. XXIV, 1087–1088.
Nittler, L., Alexander, C.M.O'D., Gao, X., Walker, R.M., Zinner, E., 1994. Interstellar oxide grains from the Tieschitz ordinary chondrite. Nature 370, 443–446.
Nittler, L.R., Amari, S., Zinner, E., Woosley, S.E., Lewis, R.S., 1996. Extinct ^{44}Ti in presolar graphite and SiC: proof of a supernova origin. Astrophys. J. 462, L31–L34.
Nittler, L.R., Alexander, C.M.O'D., Gao, X., Walker, R.M., Zinner, E., 1997. Stellar sapphires: the properties and origins of presolar Al_2O_3 in meteorites. Astrophys. J. 483, 475–495.
Nittler, L.R., Alexander, C.M.O'D., Wang, J., Gao, X., 1998. Meteoritic oxide grain from supernova found. Nature 393, 222.
Nittler, L.R., Alexander, C.M.O'D., Gallino, R., Hoppe, P., Nguyen, A., Stadermann, F., Zinner, E.K., 2008. Aluminum-, calcium- and titanium-rich oxide stardust in ordinary chondrite meteorites. Astrophys. J. 682, 1450–1478.
Nittler, L.R., Gyngard, F., Zinner, E., Stroud, R.M., 2011. Mg and Ca isotopic anomalies in presolar oxides: large anomalies in a group 3 hibonite grain. Lunar Planet. Sci. 42 abstract 1872.
Nittler, L.R., Alexander, C.M.O'D., Liu, N., Wang, J., 2018. Extremely ^{54}Cr- and ^{50}Ti-rich presolar oxide grains in a primitive meteorite: formation in rare types of supernovae and implications for the astrophysical context of solar system birth. Astrophys. J. 856, L24.
Nittler, L.R., Stroud, R.M., Alexander, C.M.O'D., Howell, K., 2020. Presolar grains in primitive ungrouped carbonaceous chondrite Northwest Africa 5958. Meteorit. Planet. Sci. 55, 1160–1175.
Nittler, L.R., Alexander, C.M.O'D., Patzer, A., Verdier-Paoletti, M.J., 2021. Presolar stardust in highly pristine CM chondrites Asuka 12169 and Asuka 12236. Meteorit. Planet. Sci. 56, 260–276.
Nollett, K.M., Busso, M., Wasserburg, G.J., 2003. Cool bottom processes on the thermally-pulsing AGB and the isotopic composition of circumstellar dust grains. Astrophys. J. 582, 1036–1058.
Nozawa, T., Kozasa, T., Habe, A., Dwek, E., Umeda, H., Tominaga, N., Maeda, K., Nomoto, K.i., 2007. Evolution of dust in primordial supernova remnants: can dust grains formed in the ejecta survive and be injected into the early interstellar medium? Astrophys. J. 666, 955–966.
Ong, W.J., Floss, C., 2015. Iron isotopic measurements in presolar silicate and oxide grains from the Acfer 094 ungrouped carbonaceous chondrite. Meteorit. Planet. Sci. 50, 1392–1407.
Palmerini, S., La Cognata, M., Cristallo, S., Busso, M., 2011. Deep mixing in evolved stars. I. The effect of reaction rate revisions from C to Al. Astrophys. J. 729, 3.
Palmerini, S., Trippella, O., Busso, M., 2017. A deep mixing solution to the aluminum and oxygen isotope puzzles in presolar grains. Mon. Not. R. Astron. Soc. 467, 1193–1201.
Palmerini, S., Cristallo, S., Busso, M., La Cognata, M., Sergi, M.L., Vescovi, D., 2021. Low mass stars or intermediate mass stars? The stellar origin of presolar oxide grains revealed by their isotopic composition. Front. Astron. Space Sci. 7, 607245.
Penzias, A.A., 1981. The isotopic abundances of interstellar oxygen. Astrophys. J. 249, 518–523.
Pignatari, M., Wiescher, M., Timmes, F.X., de Boer, R.J., Thielemann, F.-K., Fryer, C.,

Heger, A., Herwig, F., Hirschi, R., 2013. Production of carbon-rich presolar grains from massive stars. Astrophys. J. 767, L22.

Pignatari, M., Zinner, E., Hoppe, P., Jordan, C.J., Gibson, B.K., Trappitsch, R., Herwig, F., Fryer, C., Hirschi, R., Timmes, F.X., 2015. Carbon-rich presolar grains from massive stars: subsolar $^{12}C/^{13}C$ and $^{14}N/^{15}N$ ratios and the mystery of ^{15}N. Astrophys. J. 808, L43.

Podosek, F.A., Ott, U., Brannon, J.C., Neal, C.R., Bernatowicz, T.J., Swan, P., Mahan, S.E., 1997. Thoroughly anomalous chromium in Orgueil. Meteorit. Planet. Sci. 32, 617–628.

Politano, M., Starrfield, S., Truran, J.W., Weiss, A., Sparks, W.M., 1995. Hydrodynamic studies of accretion onto massive white dwarfs: ONeMg-enriched nova outbursts. Astrophys. J. 448, 807–821.

Posch, T., Kerschbaum, F., Mutschke, H., Fabian, D., Dorschner, J., Hron, J., 1999. On the origin of the 13 mu m feature. A study of ISO-SWS spectra of oxygen-rich AGB stars. Astron. Astrophys. 352, 609–618.

Priestley, F.D., Arias, M., Barlow, M.J., De Looze, I., 2022. Dust destruction and survival in the Cassiopeia A reverse shock. Mon. Not. R. Astron. Soc. 509, 3163–3171.

Qin, L., Nittler, L.R., Alexander, C.M.O'D., Wang, J., Stadermann, F.J., Carlson, R.W., 2011. Extreme ^{54}Cr-rich nano-oxides in the CI chondrite Orgueil—implication for a late supernova injection into the solar system. Geochim. Cosmochim. Acta 75, 629–644.

Rauscher, T., Heger, A., Hoffman, R.D., Woosley, S.E., 2002. Nucleosynthesis in massive stars with improved nuclear and stellar physics. Astrophys. J. 576, 323–348.

Rho, J., Kozasa, T., Reach, W.T., Smith, J.D., Rudnick, L., DeLaney, T., Ennis, J.A., Gomez, H., Tappe, A., 2008. Freshly formed dust in the Cassiopeia A supernova remnant as revealed by the Spitzer space telescope. Astrophys. J. 673, 271–282.

Rotaru, M., Birck, J.L., Allegre, C.J., 1992. Clues to early solar system history from chromium isotopes in carbonaceous chondrites. Nature 358, 465–470.

Sakamoto, N., Seto, Y., Itoh, S., Kuramoto, K., Fujino, K., Nagashima, K., Krot, A.N., Yurimoto, H., 2007. Remnants of the early solar system water enriched in heavy oxygen isotopes. Science 317, 231–233.

Singerling, S.A., Nittler, L.R., Barosch, J., Dobrică, E., Brearley, A.J., Stroud, R.M., 2023. Tracing the history of an unusual compound presolar grain from progenitor star to asteroid parent body host. Geochim. Cosmochim. Acta 344, 230–243.

Sloan, G.C., LeVan, P.D., Little-Marenin, I.R., 1996. Sources of the 13 micron feature associated with oxygen-rich circumstellar dust. Astrophys. J. 463, 310–319.

Smith, V.V., Lambert, D.L., 1990. The chemical composition of red giants. III. Further CNO isotopic and s-process abundances in thermally pulsing asymptotic giant branch stars. Astrophys. J. Suppl. 72, 387–416.

Srinivasan, G., Ulyanov, A.A., Hutcheon, I.D., Goswami, J.N., 1994. Excess ^{41}K in the early solar system. Astrophys. J. 431, L67–L70.

Straniero, O., Bruno, C.G., Aliotta, M., Best, A., Boeltzig, A., Bemmerer, D., Broggini, C., Caciolli, A., Cavanna, F., Ciani, G.F., Corvisiero, P., Cristallo, S., Davinson, T., Depalo, R., Di Leva, A., Elekes, Z., Ferraro, F., Formicola, A., Fülöp, Z., Gervino, G., Guglielmetti, A., Gustavino, C., Gyürky, G., Imbriani, G., Junker, M., Menegazzo, R., Mossa, V., Pantaleo, F.R., Piatti, D., Piersanti, L., Prati, P., Samorjai, E., Strieder, F., Szücs, T., Takács, M.P., Trezzi, D., 2017. The impact of the revised $^{17}O(p, \alpha)^{14}N$ reaction rate on ^{17}O stellar abundances and yields. Astron. Astrophys. 598, A128.

Stroud, R.M., Nittler, L.R., Alexander, C.M.O'D., 2004. Polymorphism in presolar Al_2O_3 grains from asymptotic giant branch stars. Science 305, 1455–1457.

Stroud, R.M., Nittler, L.R., Alexander, C.M.O'D., Zinner, E., 2007. Transmission electron

microscopy and secondary ion mass spectrometry of an unusual Mg-rich presolar Al_2O_3 grain. Lunar Planet. Sci. Conf. XXXVIII abstract 2203.
Stroud, R.M., Nittler, L.R., Alexander, C.M.O'D., 2008. Transmission electron microscopy of a presolar supernova hibonite grain. Lunar Planet. Sci. Conf. XXXIX abstract 1778.
Stroud, R.M., Lagos, M.J., Batson, P.E., 2018. Vibrational electron energy loss spectroscopy of astrosilicates. Microsc. Microanal. Proc. 24, 424–425.
Takigawa, A., Stroud, R.M., Nittler, L.R., Vicenzi, E.P., Herzing, A., Alexander, C.M.O.'.D., Huss, G.R., 2014a. Crystal structure, morphology, and isotopic compositions of presolar Al_2O_3 grains in unequilibrated ordinary chondrites. Lunar Planet. Sci. 45 abstract 1465.
Takigawa, A., Tachibana, S., Huss, G.R., Nagashima, K., Makide, K., Krot, A.N., Nagahara, H., 2014b. Morphology and crystal structures of solar and presolar Al_2O_3 in unequilibrated ordinary chondrites. Geochim. Cosmochim. Acta 124, 309–327.
Takigawa, A., Stroud, R.M., Nittler, L.R., Alexander, C.M.O.'.D., 2014c. A titanium oxide grain within a presolar corundum. Meteorit. Planet. Sci. 49 abstract #5389.
Takigawa, A., Stroud, R.M., Nittler, L.R., Alexander, C.M.O'D., Miyake, A., 2018. High temperature dust condensation around an AGB star: evidence from a highly pristine presolar corundum. Astrophys. J. 862, L13.
Tang, M., Anders, E., 1988. Isotopic anomalies of Ne, Xe, and C in meteorites. II. Interstellar diamond and SiC: carriers of exotic noble gases. Geochim. Cosmochim. Acta 52, 1235–1244.
Timmes, F.X., Clayton, D.D., 1996. Galactic evolution of silicon isotopes: application to presolar SiC grains from meteorites. Astrophys. J. 472, 723–741.
Trinquier, A., Birck, J.-L., Allègre, C.J., 2007. Widespread ^{54}Cr heterogeneity in the inner solar system. Astrophys. J. 655, 1179–1185.
Vangioni, E., Olive, K.A., 2019. The cosmic evolution of magnesium isotopes. Mon. Not. R. Astron. Soc. 484, 3561–3572.
Verdier-Paoletti, M.J., Nittler, L.R., Wang, J., 2019. High-resolution measurements of Mg, Si, Fe and Ni isotopes of O-rich presolar grains. 82nd Annual Meteoritical Society Meeting abstract 6433.
Vollmer, C., Hoppe, P., Brenker, F.E., 2013. Transmission electron microscopy of Al-rich silicate stardust from asymptotic giant branch stars. Astrophys. J. 769, 61.
Wanajo, S., Janka, H.-T., Müller, B., 2013. Electron-capture supernovae as origin of ^{48}Ca. Astrophys. J. 767, L26.
Wasserburg, G.J., Boothroyd, A.I., Sackmann, I.-J., 1995. Deep circulation in red giant stars: a solution to the carbon and oxygen isotope puzzles? Astrophys. J. 447, L37–L40.
Watson, D., Christensen, L., Knudsen, K.K., Richard, J., Gallazzi, A., Michałowski, M.J., 2015. A dusty, normal galaxy in the epoch of reionization. Nature 519, 327–330.
Woosley, S.E., 1997. Neutron-rich nucleosynthesis in carbon deflagration supernovae. Astrophys. J. 476, 801–810.
Woosley, S.E., Heger, A., 2007. Nucleosynthesis and remnants in massive stars of solar metallicity. Phys. Rep. 442, 269–283.
Yong, D., Lambert, D.L., Ivans, I.I., 2003. Magnesium isotopic abundance ratios in cool stars. Astrophys. J. 599, 1357–1371.
Zega, T.J., Alexander, C.M.O'D., Nittler, L.R., Stroud, R.M., 2011. A transmission electron microscopy study of presolar hibonite. Astrophys. J. 730, 83–92.
Zega, T.J., Nittler, L.R., Gyngard, F., Alexander, C.M.O'D., Stroud, R.M., Zinner, E.K., 2014. A transmission electron microscopy study of presolar spinel. Geochim. Cosmochim. Acta 124, 152–169.

Zega, T.J., Haenecour, P., Floss, C., 2020. An in situ investigation on the origins and processing of circumstellar oxide and silicate grains in carbonaceous chondrites. Meteorit. Planet. Sci. 55, 1207–1227.

Zega, T.J., Haenecour, P., Floss, C., Stroud, R.M., 2015. Circumstellar magnetite from the LAP 031117 CO3.0 chondrite. Astrophys. J. 808, 55.

Zinner, E., Amari, S., Guinness, R., Nguyen, A., Stadermann, F.J., Walker, R.M., Lewis, R.S., 2003. Presolar spinel grains from the Murray and Murchison carbonaceous chondrites. Geochim. Cosmochim. Acta 67, 5083–5095.

Zinner, E., Nittler, L.R., Hoppe, P., Gallino, R., Straniero, O., Alexander, C.M.O'D., 2005. Oxygen, magnesium and chromium isotopic ratios of presolar spinel grains. Geochim. Cosmochim. Acta 69, 4149–4165.

Zinner, E., Tang, M., 1988. Anomalous oxygen in spinels from a Murray separate. Lunar Planet. Sci. XIX, 1323–1324.